ARTICLE
https://doi.org/10.1590/2317-4889202320220041

BJGEO Brazilian Journal of Geology

Mineral chemistry and oxygen isotope studies on Sn (±W) mineralization from Pedra Branca Granite Massif, Central Brazil

Ítalo Kevin Morais dos Santos[1], Valmir da Silva Souza[1]*, Nilson Francisquini Botelho[1], Ingrid de Souza Hoyer[1], Luis Antonio Raposo Bonfim[2]

Abstract

Central Brazil hosts Paleo-Mesoproterozoic A-type granitic suites related to the Goiás Tin Province (GTP) that contain Sn (±W, Nb-Ta, REE) mineralization associated with greisen, veins, and small pegmatite bodies. The Pedra Branca granite massif (1.77–1.74 Ga) is the main representative of GTP, marked by important cassiterite (±wolframite) contents. The cassiterite contains SnO_2 = 96–100 wt. %, with the sum FeO_{total}, TiO_2, WO_3, Ta_2O_5, Nb_2O_5, In_2O_3, and UO_2 content below 4 wt.%, while wolframite contains WO_3 = 71.5–74.5 wt.%, FeO_{total} = 14.3–17.4 wt.% and MnO = 6.3–9.9 wt.%, as well as Sn, Ca, Ti, Ta, Nb, Pb, In, and U as trace elements. The $\delta^{18}O$ data on the quartz-cassiterite pair (quartz = 9.4–10.4‰, cassiterite = 2.6–2.9 ‰) from greisen reveal a magmatic-hydrothermal signature with calculated crystallization temperatures between 410 and 485°C. However, during the Neoproterozoic Brasiliano/Pan-African Orogeny (800–500 Ma), all lithologies and ore sites were subjected to flattening, fragmentation, and mylonitic deformation. Fluid inclusion data revealed the presence of low-salinity aqueous solutions with homogenization temperatures between 215 and 100°C related to Neoproterozoic deformation. Finally, during the Phanerozoic, prolonged erosive produced Sn (±W)-rich alluvium around the Pedra Branca granitic massif.

KEYWORDS: cassiterite; wolframite; Pedra Branca granite massif; Goiás Tin Province; mineral chemistry; oxygen isotope.

INTRODUCTION

Central Brazil hosts Paleo-Mesoproterozoic granitic suites, located mainly in the central-north and northeast regions of the State of Goiás (Fig. 1A), which have Sn (±W, Nb-Ta, REE) mineralization and make up the so-called Goiás Tin Province (GTP) (Marini and Botelho 1986). In general, these granite suites have petrographic and geochemical signatures similar to A-type magmatism, with a high content in alkalis, Sn, W, F, Rb, Th, Y, Nb, Ga, and REE, and often contain records of late to post-magmatic transformations, such as microclinitization, albitization, and greisenization (Botelho and Marini 1984, Marini and Botelho 1986, Botelho 1992, Botelho *et al.* 1993, Lenharo *et al.* 2002).

The Pedra Branca granite massif is the main mineralized magmatic system of the GTP (Fig. 1B). It was discovered in 1973 during a regional mineral prospecting stage carried out by the Rio Doce Geology and Mining Company, but the local was subsequently invaded by small prospectors, known as "garimpeiros" in Brazil (Jacobi 2003). The Sn (±W) concentrations occur in paleo-alluvium, greisenized granitic cupula named Bacia zone (endo- to exogreisen) and along with a greisenized NE-SW fracture/fault zone named Faixa Placha (exogreisen). Previous geological surveys carried out by mining companies estimate about 15,000 t/Sn in only 1.5 km in length from the Faixa Placha ore site (internal technical report), which have about 5 km in length. In this deposit, cassiterite occurs associated with wolframite, scheelite, arsenopyrite, chalcopyrite, sphalerite, pyrite, galena, chalcocite, stannite, and covellite (Padilha and Laguna 1981, Botelho and Marini 1984, Botelho and Rossi 1988, Botelho and Moura 1998). Despite the mineral diversity found in this deposit, investigations into the chemical composition, the stable isotopes, and the contents of the fluid inclusions in the ore minerals are still limited or nonexistent (*e.g.*, Botelho and Marini 1985, Botelho and Moura 1998, Sparrenberger and Tassinari 1999).

In this study, we analyze the chemical composition and oxygen isotopes ($\delta^{18}O$) of cassiterite, wolframite, and quartz found in the Faixa Placha ore site. Identifying the ion substitution mechanisms responsible for zonation and mineral intergrowth features, as well as the temperature and nature of the fluids will aid in the understanding of the metallogenic processes responsible for Sn (±W) mineralization at the Pedra Branca granitic massif.

ANALYTICAL PROCEDURES

The conventional petrography, electron microscopy (SEM/EDS), electron microprobe (EPMA), and fluid inclusion

[1]Geosciences Institute, Universidade de Brasília – Brasília (DF), Brazil. E-mails: italomds@hotmail.com, vsouza@unb.br, nilsonfb@unb.br, ingridshoyer@gmail.com

[2]Environment Secretary Municipal – Parauapebas (PA), Brazil. E-mail: luis_bonfim3@hotmail.com

*Corresponding author.

investigations were carried out at the Universidade de Brasília. The ore samples studied (cassiterite, wolframite, and quartz) were collected at the mining front explored by the EDEM mining company. During the SEM/EDS and EPMA analyses, the samples studied were in polished rock thin sections covered by a carbon film.

For SEM/EDS microanalysis technique, an FEI QUANTA 450 model was used, which has a high-performance EDAX Octane EDS/SDD spectrometer system, Chroma C2L cathodoluminescence imaging system for use in scanning electron microscopes (SEMs), and an EDAX DigiView electron backscatter diffraction (EBSD) camera. The imaging was acquired at a focal distance of 10 mm for 10–20 s, with a probe between 0.1 and 0.2 nm, beam current of 400–500 pA°, and an accelerating voltage of 20 kV. For the EPMA microanalysis technique, a JEOL JXA-8230 microanalyzer with five coupled wavelength dispersive spectrometers was used. The analytical conditions consisted of accelerating voltage of 20 kV, beam current of 40 nA, beam diameter of 1–2 µm, and counting times of 15 and 10 s for peak and background positions, respectively. Data reduction was performed with the ZAF program applying the specific standards of cassiterite and wolframite.

The fluid inclusion study was carried using double-polished sections (~1-mm thick) from ore samples. The conventional petrography was performed at room temperature (±25°C) with the aid of an Olympus petrographic microscope (model BX51) applying the criteria of Roedder (1984), Shepherd *et al.* (1985), and Van den Kerkhof and Hein (2001). Microthermometric data were acquired using a cooling stage and LTS420 heating from LINKAM, with a temperature range between -200 and 420°C, coupled with a petrographic microscope with long-distance objectives with magnification from 10× to 50×. The calibration was performed with H_2O-NaCl synthetic biphasic fluid inclusions, applying speed rates from 5 to 15°C/min, with an estimated accuracy of ±0.2°C for the freezing (+25 to -100°C) and ±2°C for heating (up to 350°C).

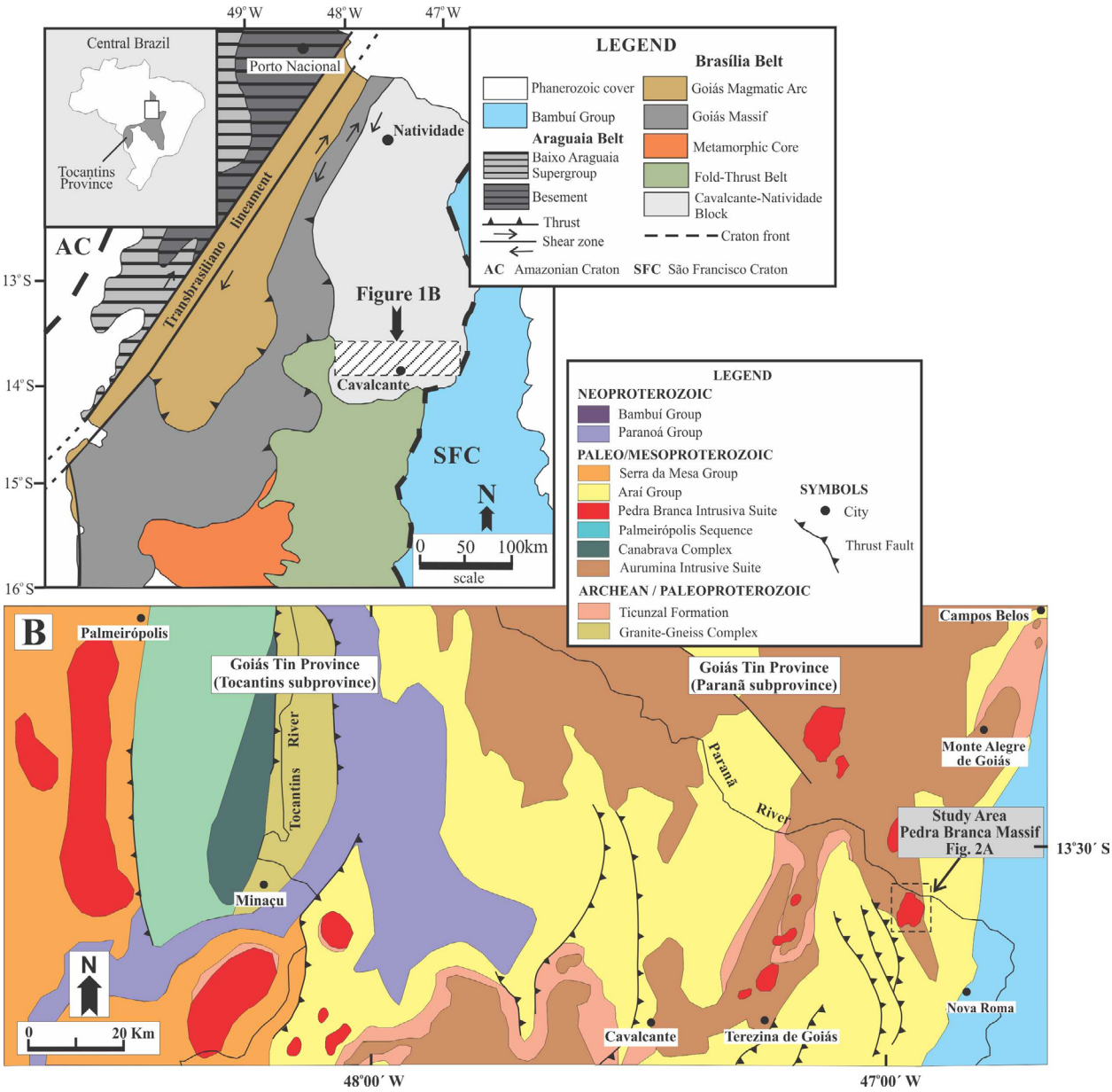

Figure 1. (A) Geological map of Central Brazil indicating the GTP location (adapted from Fuck *et al.* 2014). (B) Geological map of the GTP with highlighted study area (modified from Alvarenga *et al.* 2007).

The oxygen isotope ($\delta^{18}O$) study was carried out at the Isotope Geoscience Units of the Scottish Universities Environmental Research Centre Laboratories in Glasgow, Scotland. The oxygen isotope analyses were applied on cassiterite and quartz with a size between 0.5 and 1 cm. The nearly pure crystals samples (> 90%) were handpicked from selected specimens from the greisen. Approximately 1 mg of oxygen-bearing samples reacted with chlorine trifluoride (ClF_3) using laser heating fluorination techniques (Fallick *et al.* 1993, Macaulay *et al.* 2000). A mass spectrometer (VG SIRA 10 model) was used for the analyses, whose precision of determination from laboratory replicate analysis is 0.2‰ for $\delta^{18}O$ relative to Vienna Standard Mean Ocean Water.

GEOLOGICAL SETTING

A large part of central Brazil lies within an important regional geotectonic unit named Tocantins Province (Almeida *et al.* 1981), which brings together different tectonostratigraphic domains and subdomains that were amalgamated through thrust, nappe, and strike-slip mega-faults, under a complex tectonic architecture, occurred during the Neoproterozoic convergences and collisions between paleocontinents related to Brasiliano/Pan-African Orogeny (Uhlein *et al.* 2012, Brito Neves *et al.* 2014, Fuck *et al.* 2014, 2017, Pimentel 2016, Valeriano 2017).

The Paleo-Mesoproterozoic granitic suites from the GTP are inserted in the Brasília Belt external domain, mainly distributed in the southern part of the Cavalcante-Natividade Block (Fig. 1A). In this geological setting, the GTP brings together a set of Sn (±W, Nb-Ta, REE) specialized A-type granitic bodies, distributed in two subprovinces, named as follows (Fig. 1B):

- Tocantins subprovince to the west (Serra Dourada, Serra do Encosto e Serra da Mesa granitic massifs) intrusive in Archean-Paleoproterozoic granite-gneiss complex and Paleoproterozoic paragneiss and schists from Ticunzal Formation;
- Paranã subprovince to the east (Pedra Branca, Mocambo, Mangabeira, Mendes, Sucuri, Soledade, Teresinha, and São Domingos granitic massifs) intrusive in Archean-Paleoproterozoic Ticunzal Formation and Aurumina Suite, as well as in Paleo-Mesoproterozoic volcano-sedimentary rocks from Araí and Serra da Mesa Groups (Marini and Botelho 1986, Botelho and Rossi 1988, Marini *et al.* 1992, Botelho and Moura 1998, Teixeira and Botelho 1999, Lenharo *et al.* 2002).

Initially, these A-type granitic bodies were subdivided into two geochemical and geochronological subsuites, defined as g1 and g2 (Botelho 1992). Subsequently, these subsuites were grouped into the Pedra Branca Intrusive Suite, with the terms g1 and g2 being replaced by the terms pb1 and pb2, respectively (CPRM 2007). The older pb1 suite (aged between 1.77 and 1.74 Ga; Pimentel *et al.* 1991, Teixeira 2002) show peraluminous and alkaline geochemical affinities, high K/Na and FeOt/Mg ratio, with high Zr, Y, and REE content, and can host topaz, Li-siderofilite, quartz, or Li-fengite greisens. On the contrary, the pb2 suite (aged between 1.58 and 1.57 Ga; Pimentel *et al.* 1991, Botelho and Pimentel 1993, Sparrenberger and Tassinari 1999) shows metaluminous to peraluminous and subalkaline geochemical affinities, low K/Na and FeOt/Mg ratio, high content in SiO_2, Al_2O_3, Li, Sr, and Ta, and host fengite, quartz, and topaz greisen (Teixeira and Botelho 2002).

The Pedra Branca granite massif is inserted in the Rio Paranã subprovince (Fig. 1B). It represents the type area for the homonymous intrusive suite (CPRM 2007) and is considered one of the granitic bodies with the greatest economic potential of the GTP. It stands out in remote sensing products through its semicircular shape with about 90 km^2 of outcropping area and 1,000 m altitude over a pediplanized region around of 500 m. It was emplaced during the late Paleoproterozoic (Statherian period), intrusive in the basement Archean-Paleoproterozóic units: paragneisses, shales, and peraluminous granites from Ticunzal Formation and Auruminas Suite (> 2.15 Ga), respectively, as well as quartz-diorite to granodiorite Nova Roma (2.14 Ga). The Pedra Branca granitic plutonism occurred relatively close to voluminous Paleoproterozoic bimodal volcanism related to the early stages of the Araí intracontinental rift evolution (Arraias Formation, positioned at the basal portion of the Araí Group). However, during the Neoproterozoic Brasiliano/Pan-African Orogeny (800–500 Ma), a reasonable lithostratigraphic inversion occurred, accompanied by different deformation stages (foliation, shear zone, faults, and fractures) under low-grade metamorphic, which affected all lithologies (Pimentel *et al.* 1991, Botelho 1992, Alvarenga *et al.* 2007, CPRM 2007, Tanizaki *et al.* 2015, Martins-Ferreira 2019, Silva *et al.* 2021).

LOCAL GEOLOGY

According to Botelho (1992), five magmatic pulses, associated with pb1 and pb2 terms, are recognized in the Pedra Branca granite massif (Fig. 2). The pb1 term (1.77 Ga) gathers the less evolved magmatic pulses, represented by the following petrographic types:

- pb1b: coarse-grained porphyritic pink biotite granite;
- pb1c: coarse-grained porphyritic to inequigranular pink biotite granite.

On the contrary, the pb2 term (1.74 Ga) brings together the more evolved/fractionated magmatic pulses:

- pb2b: partially albitized coarse-grained inequigranular pink biotite granite;
- pb2c: albitized medium-grained equigranular pink biotite granite;
- pb2d: albitized and greisenized Li-mica leucogranite.

Additionally, the pb2 term also associates metric porphyritic dykes, as well as wide and irregular greisen aureole surrounding the pb2d petrographic type.

The Sn (±W) mineralization is linked to the most evolved magmatic pulse from pb2 term, represented by Li-mica leucogranite or pb2d petrographic type, associated to greisen

bodies, distributed in the main greisen sector named "Bacia zone" and along with the "Faixa Placha" (Fig. 2). The Bacia zone hosts several irregular endogreisen bodies, as well as quartz-veins and some pegmatites small bodies. This place presents a concave geomorphology, formed from partial erosion of the granitic cupola (Fig. 3A), which favored the concentration and distribution of Sn (±W) mineralization to the drainage network located below the Pedra Branca massif, thus contributing to the discovery of this mineral deposit (e.g., Jacobi 2003). On the contrary, the Faixa Placha is a NE-SW linear and subvertical structure formed by greisenized tensile fractures/faults sets or exogreisen (Figs. 2 and 3B), probably generated or reopened during the intrusion of the pb2 magmatic phase. However, during Brasiliano/Pan-African Orogeny, this structure was then reactivated under a ductile-brittle regime and with sinistral cinematic (shear fault regime), favoring flattening, fragmentation, and partial mylonitic deformation on the lithologies. Lenticular greisen bodies, quartz veins-veinlets, greisen-filled tensile fractures/fissures, some breccia, and tension gashes also are observed in that ore site (Figs. 3C and 3D).

The Faixa Placha is the main ore site in the Pedra Branca granite massif. Herein, the greisenized granite has around Sn = 50 ppm, which gradually increases toward the Faixa Placha, reaching around Sn = 2,000 ppm (Botelho and Marini 1984, 1985, Botelho and Rossi 1988). Previous studies on mineral chemistry (EPMA microanalysis technique) indicate anomalous contents of indium (In = 1,500 ppm) in cassiterite, sphalerite, and stannite, which can be extracted in metallurgical

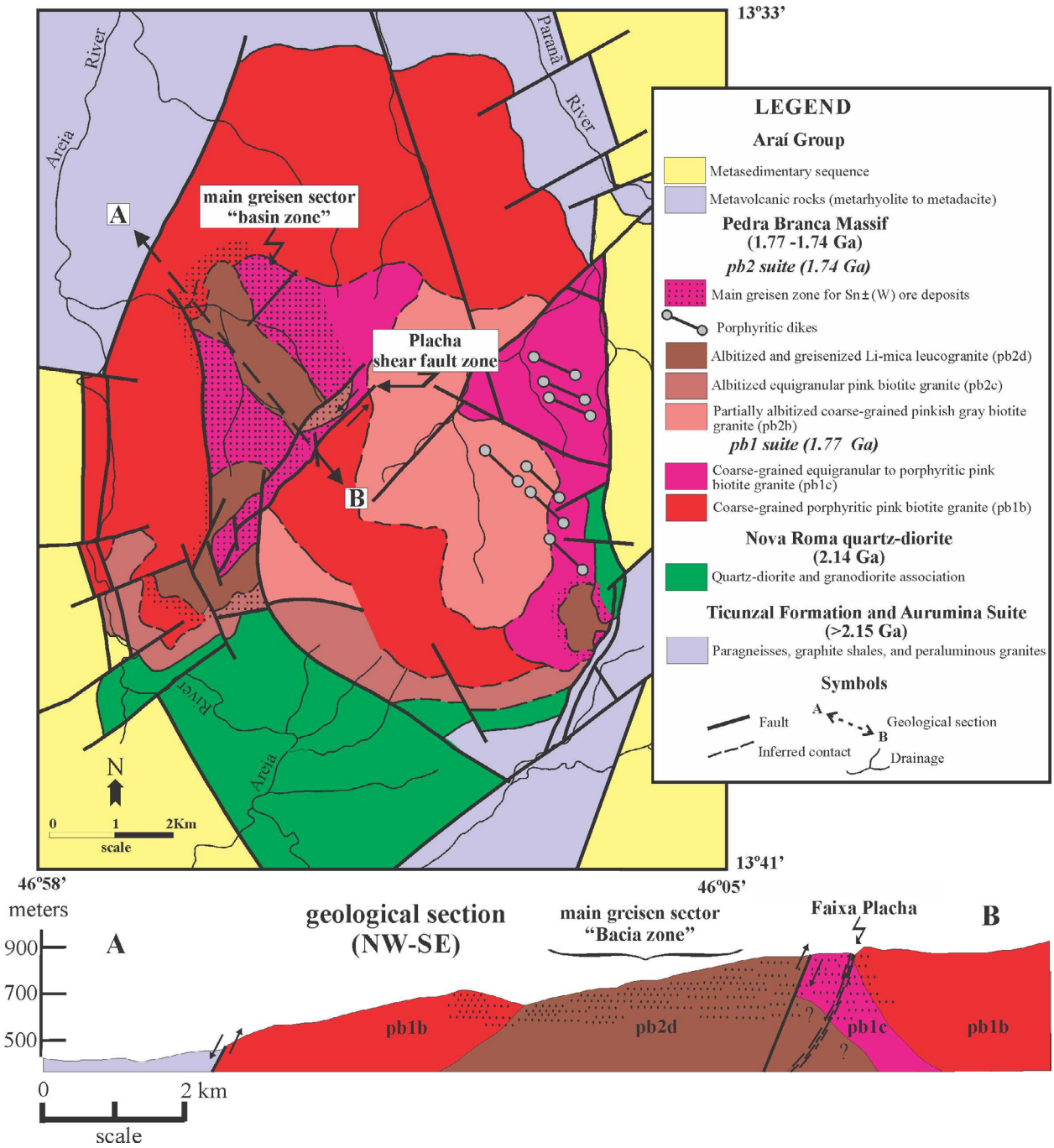

Source: modified from Botelho and Rossi (1988) and Botelho (1992).

Figure 2. (A) Geological map of the Pedra Branca granite massif with emphasis on the A–B geological section, indicating the Bacia zone and the Faixa Placha ore sites.

treatment, adding thus economic value to the deposit (Botelho and Moura 1998). Additionally, geophysical investigations indicate the highest magnetic, U and Th anomalies at a depth of around 350 m (Carvalhêdo *et al.* 2020), while geochemical investigations point to high REE-Y concentrations in this place (Marini *et al.* 1992, Costa *et al.* 2020). In general, along the Faixa Placha ore site, cassiterite (±wolframite) crystals occur disseminated or in centimetric to metric podiform-shaped aggregates, frequently associated with fluorite, arsenopyrite, chalcopyrite, ilmenite, magnetite, hematite, scheelite, sphalerite, pyrite, galena, chalcocite, stannite, and covellite, encapsulated in topaz-mica-quartz greisen, mica-quartz greisen, and mica greisen bodies or quartz veins-veinlets (Botelho and Marini 1984, 1985, Botelho and Rossi 1988).

PETROGRAPHIC AND MINERAL CHEMISTRY DATA

These data were obtained from ore samples encapsulated in greisenized tensile fractures/faults sets (exogreisen) of the Faixa Placha site, whose results are presented below.

Cassiterite

The euhedral to subhedral cassiterite crystals are zoned, slightly to moderately fractured containing microinclusions of ilmenite, rutile, tantalite, and magnetite. Pleochroism is weak in lighter varieties and medium to strong in darker varieties. In general, its typical zoning is marked by alternating bands of pale yellow, orange, light brown, to dark brown (Figs. 4A and 4B). However, in the Faixa Placha ore site, some greisen bodies, as well as tensile and shear fractures/fissures, have cassiterite crystals broken and sometimes stretched as a result of the deformation related to the Brasiliano/Pan-African Orogeny (Figs. 4C and 4D).

The cassiterite has SnO_2 contents between 96.2 and 99.7 wt.%, while the sum of the other elements analyzed has content below 4 wt.% (Table 1). FeO_{total}, TiO_2, and WO_3 are the main impurities, while Ta_2O_5, Nb_2O_5, In_2O_3, and UO_2 appear as trace elements. The colors of lesser intensity, ranging from dark yellow, orange, to light brown, have higher contents in SnO_2 and lower in FeO_{total}, TiO_2, Ta_2O_5, Nb_2O_5, WO_3, In_2O_3, and UO_2. On the contrary, the zones whose colors vary from dark red to dark brown have a lowered SnO_2 content accompanied by a relative increase FeO_{total}, TiO_2, and WO_3. These geochemical characteristics corroborate with what is already known in the literature regarding the chemical composition of zoned cassiterites from other deposits in the world (Giuliani 1987, Neiva 1996, Murciego *et al.* 1997, Costi *et al.* 2000, Souza and Botelho 2009, Nascimento and Souza 2017).

Chemical variations in zoned cassiterites have been attributed to physicochemical parameters changes (pressure, temperature, fO_2, pH, and Eh) during the nucleation and crystal growth over the magmatic-hydrothermal system evolution (e.g., Neiva 1996, 2008, Murciego *et al.* 1997, Möller *et al.* 1988, Souza and Botelho 2009, Nascimento and Souza

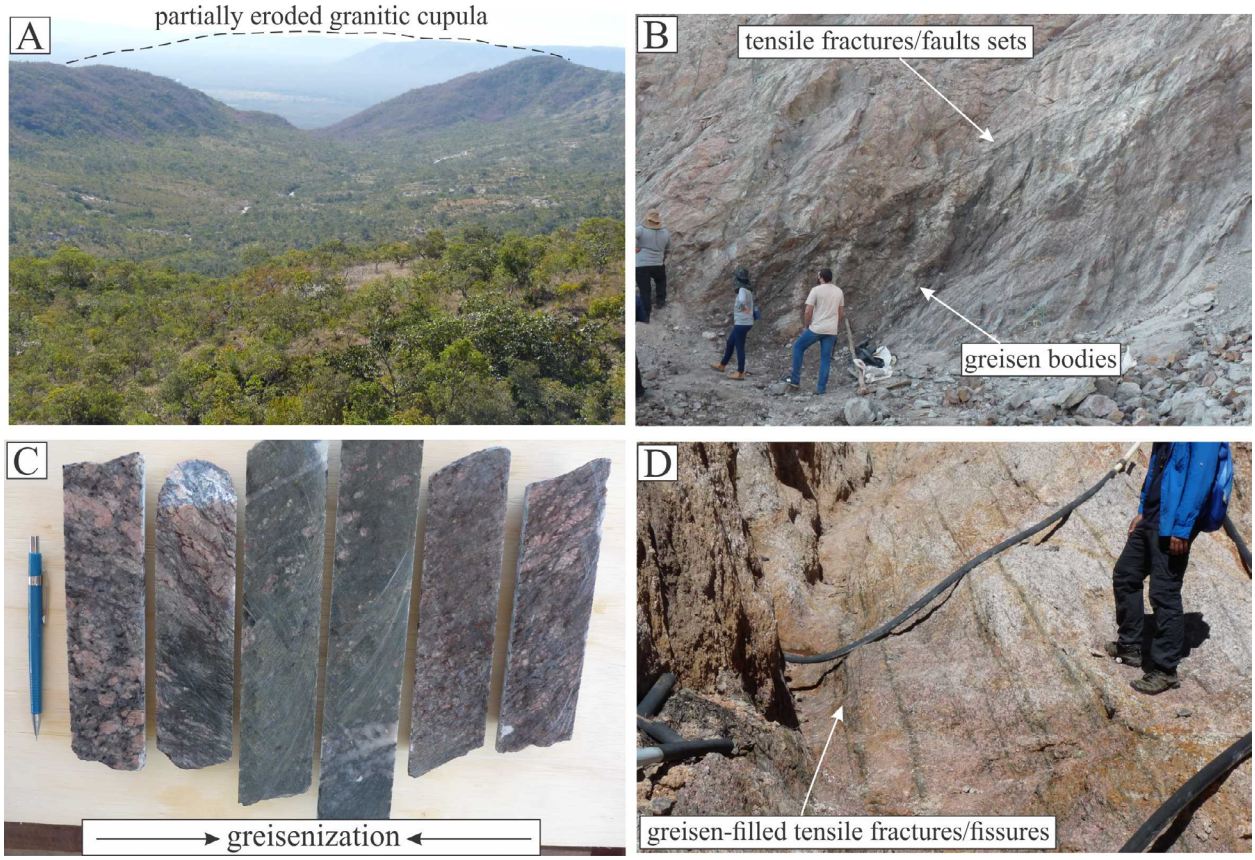

Figure 3. General aspects of ore sites in the Pedra Branca granite massif: (A) Northwest panoramic view of the Bacia zone with a dashed line indicating the probable outline of the partially eroded granitic cupula; (B) partial view of the mining front in the Faixa Placha. Observe the NE-SW tensile fractures/faults sets, as well as the lenticular greisen bodies; (C) drill-cores set from Faixa Placha ore site showing the greisenization on the deformed coarse-grained pink porphyritic biotite granite (pb1b petrographic type); (D) greisen-filled tensile fractures/fissures sets in the Faixa Placha ore site.

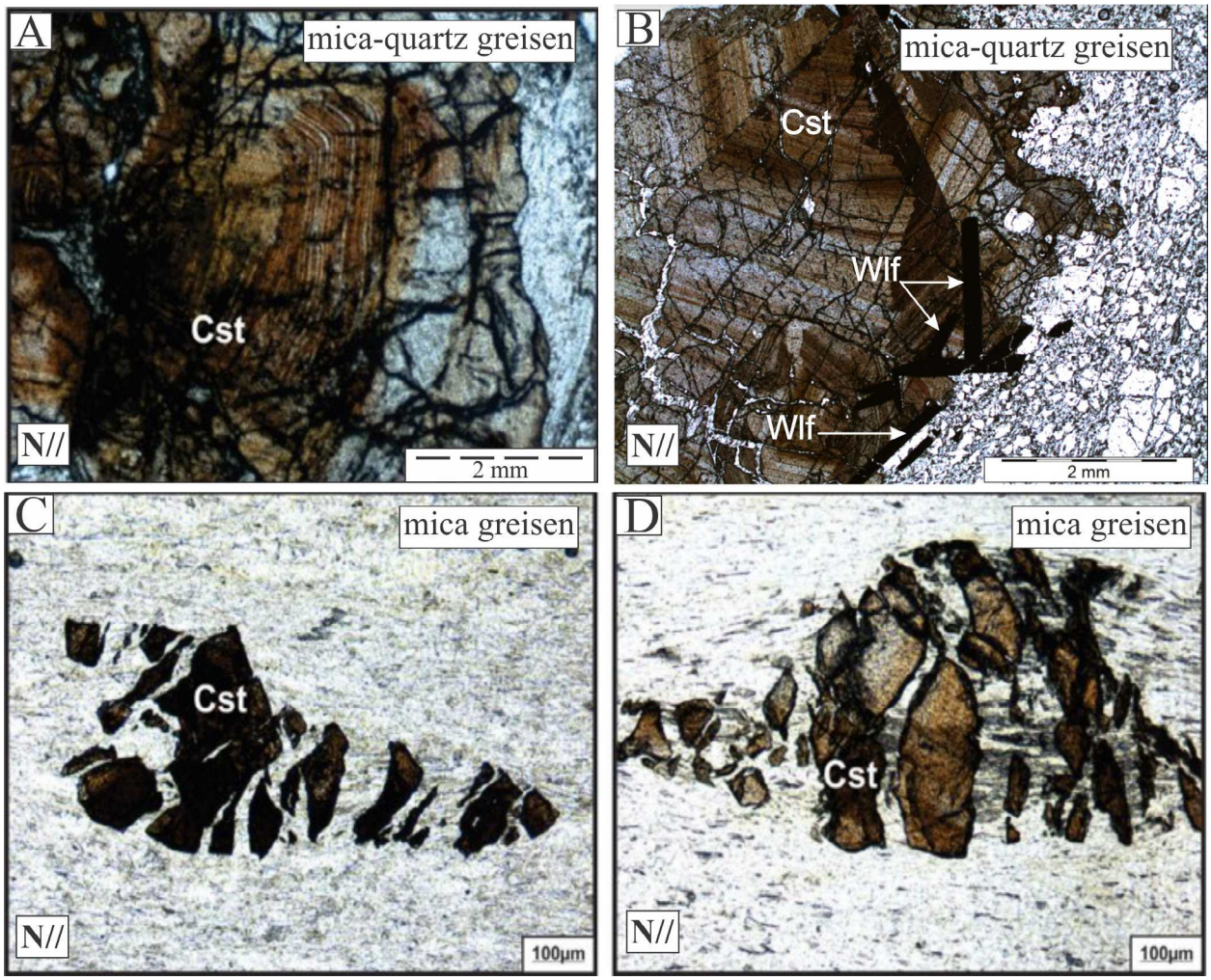

Figure 4. Photomicrographs of cassiterite (Cst) and wolframite (Wlf) crystals in greisen from Faixa Placha ore site (N// = parallel nicois). (A, B) Note the typical zoning and partially fracturing of cassiterite crystals as well as the tabular wolframite crystals associated in mica-quartz greisen. (C, D) Cassiterite crystals broken and stretched in mica greisen.

Table 1. Electron microprobe analysis results on cassiterite crystals. The composition of oxides in percent by weight (wt.%) and of element in atoms per formula unit (apfu) calculates on the basis of two oxygens. The symbol (–) represents values below the detection limit.

	Cassiterite																			
Spots	1	2	3	4	5	6	7	8	9	10	11	12	13	14	15	16	17	18	19	20
SnO_2	99.05	98.19	98.48	96.24	97.58	98.78	98.24	97.02	97.29	99.00	99.35	98.77	98.57	98.98	99.01	98.97	98.65	99.66	98.44	99.64
$FeO_{tot.}$	0.26	0.17	0.05	0.56	1.00	0.31	0.46	0.27	0.35	0.32	0.23	0.07	0.02	0.14	0.06	0.1	0.07	0.03	0.07	0.10
TiO_2	0.20	0.17	0.2	0.33	0.56	0.38	0.55	0.50	0.59	0.16	0.17	0.15	0.18	0.07	0.13	0.16	0.11	0.07	0.26	0.05
MnO	–	–	0.01	–	0.03	–	0.02	0.03	0.04	–	–	0.01	–	0.02	–	–	0.05	0.02	0.02	–
WO_3	0.02	0.26	0.64	0.6	–	–	–	0.90	0.94	–	–	0.62	0.63	0.75	0.3	0.5	0.7	–	0.27	0.04
Ta_2O_5	0.05	0.05	–	0.15	0.05	0.03	0.06	0.10	0.15	–	–	–	0.12	0.09	0.09	0.09	0.03	0.1	0.07	0.09
Nb_2O_5	0.02	0.53	0.12	2	0.06	0.09	–	0.63	0.60	–	–	–	–	0.11	0.01	–	–	0.17	0.20	0.09
PbO	0.01	–	0.01	–	0.06	–	–	–	0.01	–	0.02	–	0.01	0.07	0.01	0.05	–	–	–	–
In_2O_3	–	0.02	–	0.03	–	0.01	0.03	0.03	0.04	0.01	0.02	0.04	0.05	0.06	–	–	0.02	–	–	–
UO_2	0.02	0.01	–	0.04	0.04	–	–	–	–	–	0.03	–	–	–	–	–	–	–	0.01	–
Total	**99.63**	**99.40**	**99.51**	**99.59**	**99.60**	**99.6**	**99.36**	**99.48**	**100.01**	**99.49**	**99.82**	**99.66**	**99.58**	**100.29**	**99.61**	**99.87**	**99.63**	**100.05**	**99.34**	**100.01**
Sn	0.993	0.986	0.989	0.957	0.979	0.989	0.986	0.972	0.969	0.994	0.995	0.991	0.990	0.988	0.994	0.991	0.991	0.995	0.989	0.996
Fe	0.005	0.003	0.001	0.010	0.019	0.006	0.009	0,005	0.007	0.006	0.004	0.001	–	0.003	0.001	0.002	0.001	0.001	0.001	0.002
Ti	0.003	0.003	0.003	0.006	0.009	0.006	0.009	0.008	0.010	0.003	0.003	0.003	0.003	0.001	0.002	0.003	0.002	0.001	0.004	0.001
Mn	–	–	–	–	0.001	–	–	0.001	0.001	–	–	–	–	–	–	–	0.001	–	–	–
W	–	0.002	0.004	0.003	–	–	–	0.005	0.005	–	–	0.004	0.004	0.004	0.002	0.003	0.004	–	0.002	–
Ta	–	–	–	0.001	–	–	–	0.001	0.001	–	–	–	0.001	0.001	0.001	0.001	–	0.001	–	0.001
Nb	–	0.005	0.001	0.020	0.001	0.001	–	0.006	0.006	–	–	–	–	0.001	–	–	–	0.002	0.002	0.001
Pb	–	–	–	–	–	–	–	–	–	–	–	–	–	–	–	–	–	–	–	–
In	–	–	–	–	–	–	–	–	–	–	–	–	–	0.001	–	–	–	–	–	–
U	–	–	–	–	–	–	–	–	–	–	–	–	–	–	–	–	–	–	–	–
Total	**1.001**	**0.999**	**0.998**	**0.998**	**1.010**	**1.003**	**1.004**	**0.999**	**0.999**	**1.003**	**1.002**	**0.999**	**0.998**	**0.999**	**1.000**	**0.999**	**0.999**	**1.000**	**0.999**	**1.000**

2017). According to these authors, the replacement of Sn by Fe+Ti impurities can be described by $2Sn^{4+} + O^{2+} \leftrightarrow Ti^{4+} + Fe^{3+} + OH^{-}$, which was responsible for oscillation in the colors (zoning) of the cassiterite and can be illustrated through the Sn versus Fe+Ti correlation diagram (Fig. 5A). However, other coupled substitutions linked to different oxidation states of Fe can be described by $3(Sn, Ti)^{4+} \leftrightarrow 2(Nb, Ta)^{5+} + (Fe, Mn)^{2+}$ and $2(Sn, Ti)^{4+} \leftrightarrow (W, Mn)^{6+} + Fe^{2+}$, involving the other elements or geochemical impurities identified, which can be observed through the Sn+Ti versus Fe+Mn+W+Nb+Ta correlation diagram (Fig. 5B).

In general, the darker zones have more Ti than the lighter zone, indicating the effective substitute $Sn^{4+} \leftrightarrow Ti^{4+}$ associated with higher content of inclusions or exsolutions of titanium oxide minerals (rutile and ilmenite). According to Neiva (1996), the mechanism of incorporation of Fe, Mn, W, Nb, and Ta in the Ti-darker zones can be explained by equations $2(Nb, Ta)^{5+} + (Fe, Mn)^{2+} \leftrightarrow 3Ti^{4+}$ and $(Mn, W)^{6+} + Fe^{2+} \leftrightarrow 2Ti^{4+}$. The regular decrease in Ti as Fe+Mn+Nb+Ta increases also indicates that the mechanism $(Nb, Ta)^{5+} + Fe^{3+} \leftrightarrow 2Ti^{4+}$ might have operated. The increase of W+Mn+Fe in Ti-rich darker zones can indicate the formation of a specie of metastable molecular wolframite in these sites, marked by substitution of Sn_2O_4 by $(Fe,Mn)WO_4$ (according to Möller *et al.* 1988, Neiva 2008).

The irregular anomalous contents (100–700 ppm) of In and U in the cassiterite structure are also associated with Fe-Ti darker zones, indicating the important mechanism of substitution of Sn by Fe+Ti on the coupled incorporation of other chemical impurities, as suggested by the equations $2(Sn, Ti)^{4+} \leftrightarrow (Nb, Ta)^{5+} + (Fe, In)^{3+}$ or $2(Sn, Ti)^{4+} \leftrightarrow U^{4+} + 2Fe^{2+}$.

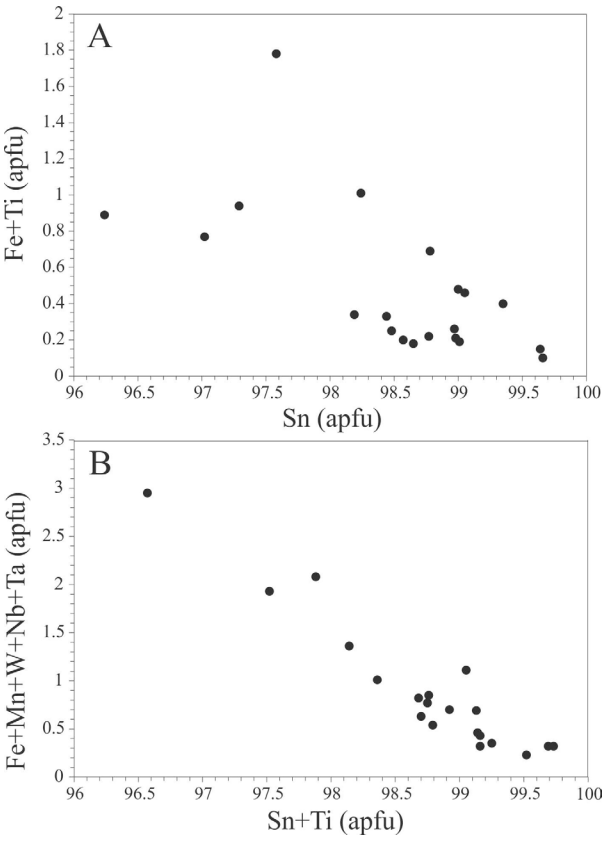

Figure 5. Atomic (apfu) correlation diagrams applied for cassiterite crystals from the Faixa Placha ore site. (A) Sn versus Fe+Ti; (B): Sn+Ti versus Fe+Mn+W+Nb+Ta.

Wolframite

Wolframite crystals are relatively rarer and occur disseminated in greisen and veins, normally associated with cassiterite crystals (Fig. 4B). It displays opaque euhedral to subhedral crystals and tabular in shape, but can also occur in small massive aggregates (Fig. 6A), often with a wide range of a size (500–8,000 µm). Wolframite crystals commonly host niobium-tantalate and ilmenite as microinclusions or exsolutions (Figs. 6B and 6C).

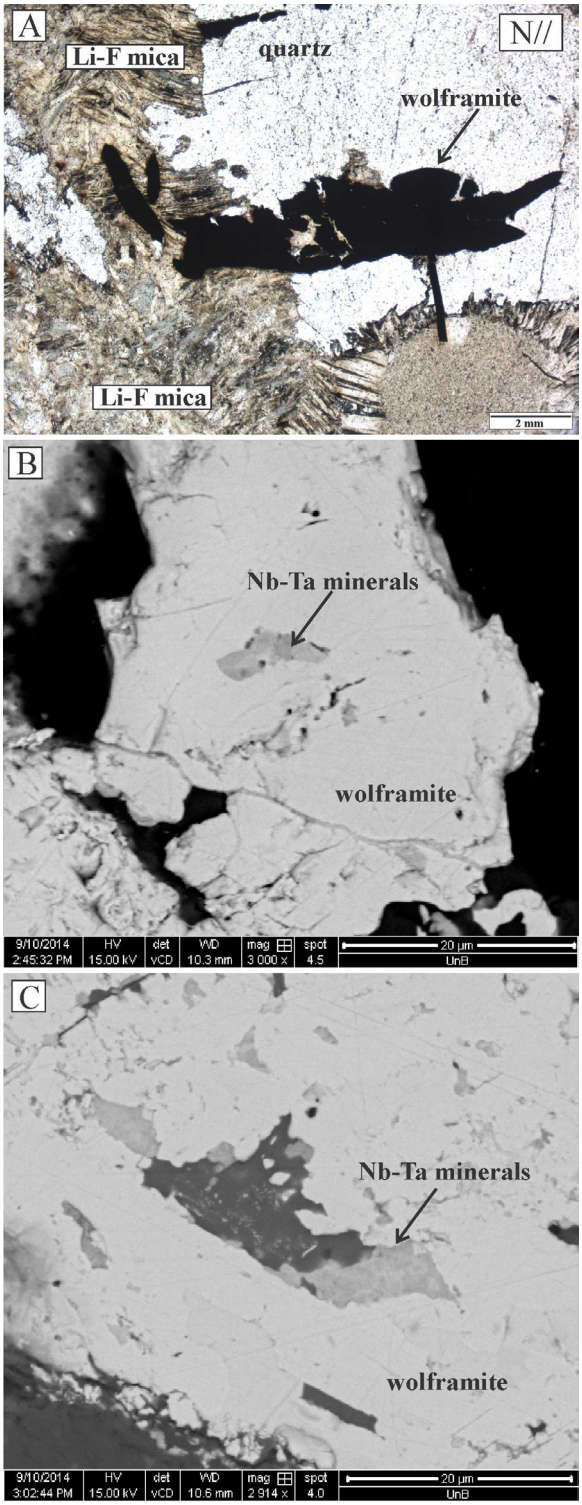

Figure 6. Microscopic features of the wolframite crystals from Faixa Placha ore site. (A) Photomicrography of the wolframite aggregate crystals in quartz-mica greisen (N// = parallel nicois); (B, C) scanning electron microscope (SEM) images on wolframite with niobium-tantalates mineral species as microinclusions or exsolutions.

The chemical analyses revealed that the wolframite from the Faixa Placha ore site has WO_3 content from 71.5 to 74.5 wt.%, followed by FeO_{total} = 14.3–17.4 wt.% and MnO = 6.3–9.9 wt.%, as well as Sn, Ca, Ti, Ta, Nb, Pb, In, and U as trace elements (Table 2). Wolframite has structural formula expressed by AWO_4, where A = Fe, Mn, forming a complete solid solution represented by ferberite ($FeWO_4$) and hubnerite ($MnWO_4$) as endmembers (Hsu 1976, Waychunas 1991, Macavei and Schulz 1993, Neiva 2008). The FeO_{total} content is almost twice the MnO content, whose spots set form trends plotted in the ferberite field (Fig. 7A). Therefore, the structural formula of the wolframite studied can be defined as ($Fe_{0.61-0.74}$ – $Mn_{0.27-0.42}$) WO_4, with Nb_2O_5 appearing as the main impurity (content = 0.2–2.2 wt.%), while SnO_2, CaO, TiO_2, Ta_2O_5, PbO, In_2O_3, and UO_2 present contents below 0.25 wt.% (Fig. 7B).

The Nb and Ta incorporation (niobium-tantalate species) like a kind of solid solution in the wolframite structure may result from coupled substitutions, expressed by the equation $Fe^{2+} + W^{6+} \leftrightarrow Fe^{3+} + (Nb, Ta)^{5+}$, which can favor zoning on (Fe, Mn)(W, Nb, Ta)O_4 mineral specie (Polya 1988, Tindle and Webb 1989, Neiva 2008). This mechanism of substitution also favors the decrease of W^{6+} versus $(Nb + Ta)^{5+}$ increases, with the electrostatic charge deficiency resulting in the iron oxidation $Fe^{2+} \leftrightarrow Fe^{3+}$ (Neiva 2008). According to Harlaux *et al.* (2018), the isovalent substitution $Fe^{2+} \leftrightarrow Mn^{2+}$ in octahedral coordination has a nonlinear trend and leads to a minor excess in Fe^{3+} into the structure of wolframite.

This mechanism can be observed by negative correlation of Fe versus Mn (Fig. 7C), corresponding to the isovalent substitution of $Fe^{2+} \leftrightarrow Mn^{2+}$, or by a regular decrease in W followed by an increase of Nb+Ta at the wolframite structure from the Faixa Placha ore site (Fig. 7D). The decrease in W^{6+} is also flowed by irregular increases of Sn^{4+}, In^{3+}, and U^{4+}, which may also be linked to accidental microinclusions and exsolutions, or as a result of $2Fe^{2+} + W^{6+} \leftrightarrow 2(Fe, In)^{3+} + (Sn, U)^{4+}$ coupled substitutions.

OXYGEN ISOTOPE DATA ($\delta^{18}O$)

Oxygen isotopic data have been widely applied to mineral pairs focusing on the source and geothermometry of magmatic-hydrothermal systems (e.g., Kelly and Rey 1979, Zhang *et al.* 1994, Taylor Jr. 1997, Crowe *et al.* 2001, Faure and Mensing 2004, Mering *et al.* 2018). We obtained $\delta^{18}O$ data on the quartz-cassiterite pair under association paragenetic encapsulated in mica-quartz greisen bodies from the Faixa Placha ore site, whose results are presented below.

Table 2. Electron microprobe analysis results on wolframite crystals. Compositions of oxides in percent by weight (wt.%) and of elements in atoms by unit formula (apfu), calculates on the basis of four oxygens. The symbol (–) represents values below the detection limit.

	Wolframite									
Spots	**1**	**2**	**3**	**4**	**5**	**6**	**7**	**8**	**9**	**10**
SnO_2	0.07	0.23	–	–	–	–	–	0.04	0.72	0.02
CaO	0.08	0.06	0.04	0.01	0.02	0.02	0.05	0.05	0.07	0.03
FeO	17.44	14.43	15.47	14.99	15.27	16.91	14.91	14.41	15.31	15.63
TiO_2	0.05	0.04	0.02	0.01	0.05	0	0.02	0	0.05	0.07
MnO	6.30	9.43	9.06	9.21	8.73	7.43	9.18	9.87	8.94	9.21
WO_3	72.81	71.55	74.24	73.21	73.73	73.62	73.76	71.8	71.85	73.67
Ta_2O_5	0.10	0.11	0.06	0.07	0	0.06	0.05	0.17	0.18	0.11
Nb_2O_5	1.13	2.28	0.29	0.78	0.45	0.78	0.57	1.71	1.83	1.02
PbO	0.02	0.02	–	–	–	–	0.02	–	–	–
In_2O_3	0.04	0.06	0.03	–	–	–	0.03	0.01	0.03	0.02
UO_2	0.03	0.05	–	0.07	–	–	–	–	0.06	0.05
Total	**98.06**	**98.26**	**99.21**	**98.35**	**98.25**	**98.82**	**98.59**	**98.06**	**99.04**	**99.83**
Sn	0.001	0.005	–	–	–	–	–	–	0.014	–
Ca	0.004	0.003	–	–	0.002	0.001	0.003	0.003	0.003	0.002
Fe	0.745	0.613	0.657	0.641	0.654	0.719	0.636	0.615	0.647	0.657
Ti	0.002	0.001	–	–	0.002	–	–	–	0.002	0.003
Mn	0.273	0.406	0.39	0.401	0.378	0.32	0.397	0.427	0.382	0.392
W	0.966	0.942	0.977	0.97	0.979	0.971	0.976	0.95	0.94	0.96
Ta	0.001	0.001	0.01	0.001	–	0.001	0.001	0.002	0.002	0.001
Nb	0.026	0.052	0.007	0.018	0.01	0.018	0.013	0.04	0.042	0.023
Pb	–	–	–	–	–	–	–	–	–	–
In	–	–	–	–	–	–	–	–	–	–
U	–	–	–	–	–	–	–	–	–	–
Total	**2.018**	**2.023**	**2.041**	**2.031**	**2.025**	**2.03**	**2.026**	**2.037**	**2.032**	**2.038**
Fe^{3+}	0.034	0.057	0.023	0.03	0.021	0.023	0.024	0.051	0.06	0.04
Fe^{2+}	0.696	0.527	0.622	0.596	0.622	0.675	0.599	0.537	0.557	0.597

Quartz ($\delta^{18}O$ = 9.4–10.4‰) and cassiterite ($\delta^{18}O$ = 2.6–2.9‰) have subtle variations in their respective isotopic compositions, indicating isotopic equilibrium with a common magmatic-hydrothermal system (Table 3). Otherwise, significant differences in $\delta^{18}O$ values between quartz-cassiterite reveal the mineral isotopic fractionation signatures during the rise of the hydrothermal system (Alderton 1989, Burnham 1997, Taylor Jr. 1997). In general, cassiterite from Sn-W magmatic-hydrothermal deposits typically record low $\delta^{18}O$ values ($\delta^{18}O$ < 10‰), due to its greater sensitivity to isotopic fractionation, which have been attributed to the temperature drop during a mixing phase between meteoric fluids (isotopically light) and magmatic fluids (Kelly and Rye 1979, Jackson and Helgeson 1985, Sun and Eadington 1987, Taylor and Wall 1993, Heinrich *et al.* 1996). In contrast, quartz often records higher $\delta^{18}O$ values ($\delta^{18}O$ ~ 10 ‰) due to its low sensitivity to isotopic changes in the hydrothermal system (Clayton *et al.* 1972, Taylor Jr. 1997, Sharp *et al.* 2016).

We used $\delta^{18}O$ data from the quartz-cassiterite pair in the geothermometric study of the Pedra Branca magmatic-hydrothermal system. The geothermometric calculations were made based on the fractionation curve given by $1{,}000 \ln\alpha = 1.259 \times 10^6 / T^2 + 8.15 \times 10^3 / T - 4.72$ and $1{,}000 \ln\alpha = 2.941 \times 10^6/T^2 - 11.45 \times 10^3/T + 4.72$ (Li *et al.* 2022), as well as $1{,}000 \ln\alpha = 3.38 \times 10^6 / T^2 - 3.40$ (Clayton *et al.* 1972), applied to the quartz-cassiterite-water system. Considering that cassiterite and quartz are in paragenetic association, we then obtained the geothermometric range calculated from 410 to 485°C, applying a correlation between the different quartz $\delta^{18}O$ values (9.4–10.4‰) for each cassiterite $\delta^{18}O$ value (2.6–2.9‰) in order to obtain an isotopic range, which we interpret as the temperature range for ore crystallization during the evolution of the Pedra Branca magmatic-hydrothermal system. This isotopic temperature range has also been recorded in other Sn-W deposits around the world linked to the Sn-specialized granitic magmas evolution (e.g., Linnen and Williams-Jones 1995, Bettencourt *et al.* 2005, Macey and Harris 2006, Li *et al.* 2021).

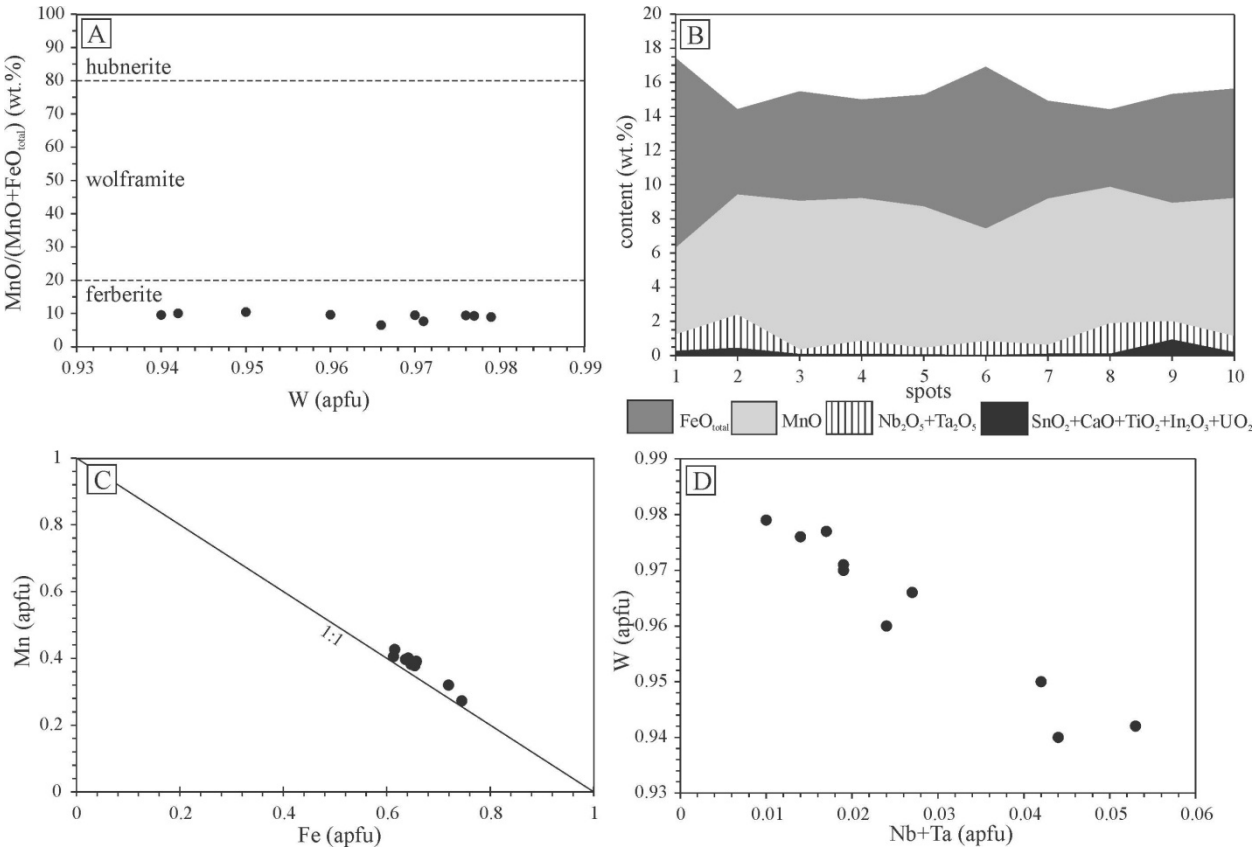

Figure 7. (A) MnO/(MnO+Fe_{total}) versus W discriminant diagram applied for wolframite classification (adapted from Yang *et al.* 2020); (B) electron microprobe spots set showing the variation in the wolframite compositional content; (C) Negative correlation Mn versus Fe indicative for isovalent substitution ($Fe^{2+} \leftrightarrow Mn^{2+}$); (D) W versus Nb+Ta correlation diagram indicating the main substitution mechanism in the wolframite ($Fe^{2+} + W^{6+} \leftrightarrow Fe^{3+} + (Nb, Ta)^{5+}$).

Table 3. Oxygen isotope ($\delta^{18}O$) values obtained for cassiterite and quartz samples from mica-greisen of the Faixa Placha ore site with their calculated isotopic temperature ranges.

Sample	Mineral	$\delta^{18}O$ (‰)	Mineral Pair	Temperature (°C)
G-1202111	Cassiterite	2.7	Cassiterite + quartz	413–484
G-1202112	Cassiterite	2.9		
G-1202113	Cassiterite	2.6	Cassiterite + quartz	427–498
G-1202114	Quartz	9.4		
G-1202115	Quartz	9.7	Cassiterite + quartz	406–477
G-1202116	Quartz	10.4		

FLUID INCLUSION DATA

Fluid inclusion studies also have been widely applied in the physicochemical characterization (composition, temperature, and pressure) of the magmatic-hydrothermal system (e.g., Chang *et al.* 2018, Daele *et al.* 2018, Audétat 2019). In this study, we present fluid inclusion data obtained on deformed quartz and cassiterite crystals from mica-quartz greisen bodies of the Faixa Placha ore site (Figs. 8A and 8B). The results are presented and discussed below.

The quartz and cassiterite crystals often occur broken and stretched in this ore site, but quartz still exhibits different stages of recrystallization, features that are not clearly observed in cassiterite. They host, at 25°C room temperature, monophasic and biphasic aqueous fluid inclusions, characterized as pseudo-secondary and secondary types (Figs. 8C–8F). The pseudo-secondary type occurs isolated or in small groups on trails, displays irregular, elongated, and subrounded shapes, with 5–60 µm in size. The secondary type form trails along healed microfractures, with elongated and rounded shapes, but with a size below 5 µm, thus making it impossible to obtain microthermometric data in the equipment used.

The biphasic (H_2O_{liq} + H_2O_{gas}) pseudo-secondary type has a gas phase volume (Vg/V_{total}) estimated between 5 and 10%, while the monophasic pseudo-secondary type can have a liquid or gas phase, filling the entire cavity (Figs. 8C–8F). The microthermometry results are summarized in Table 4.

- Cassiterite: The melting first occurs at the eutectic temperature (Te) between -36.4 and -22.3°C. Although Te measurements have normally limited accuracy, this microthermometric range obtained suggests the presence of Na, K, Mg, and Fe ions in this aqueous solution (Shepherd *et al.* 1985, Bodnar 1993, Bodnar and Vityk 1994). The melting ice temperature (Tmi) occurred between -10.4 and -8.2°C (Fig. 9A), indicating a calculated salinity from 14 to 12 wt.%

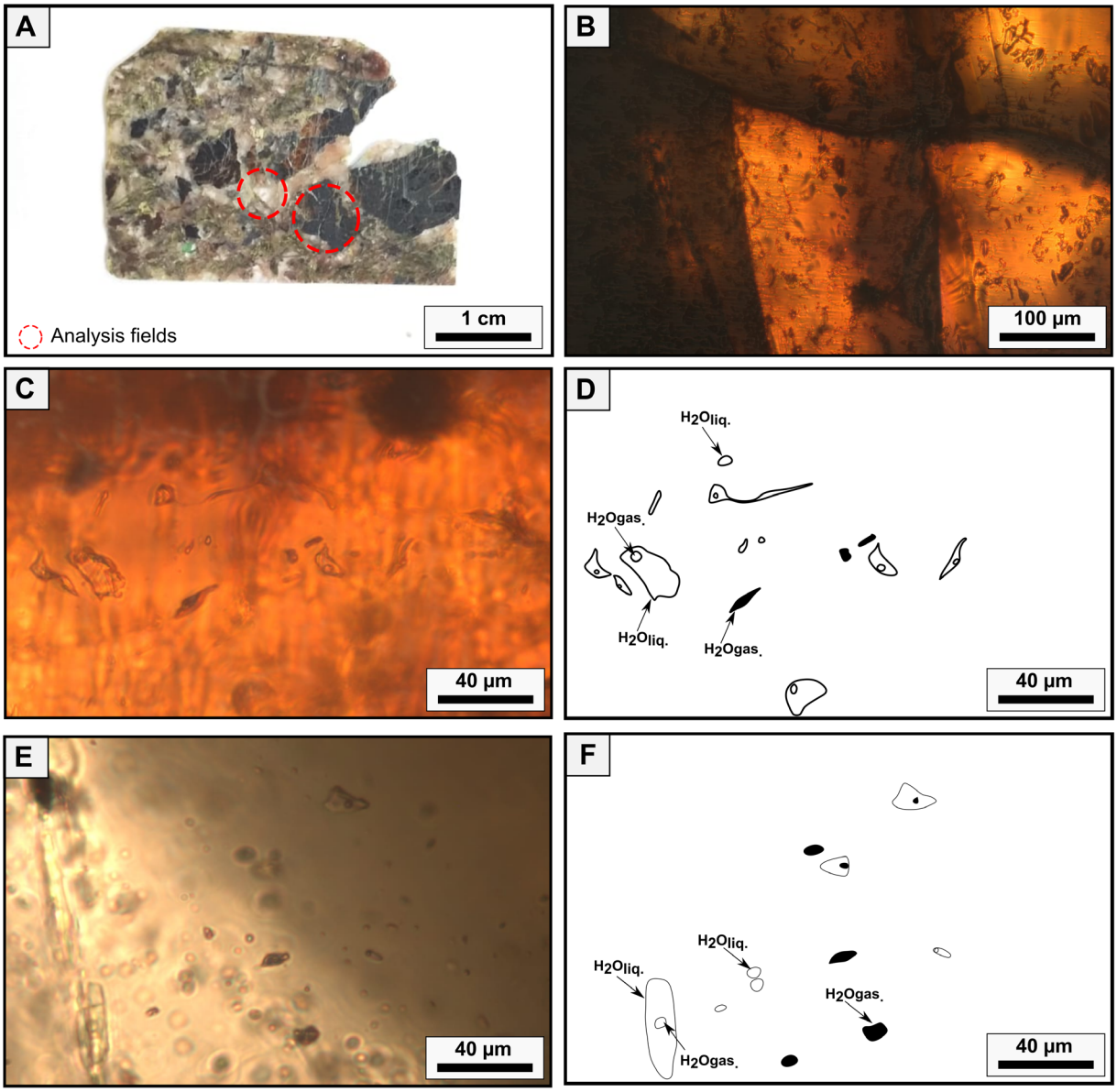

Figure 8. Morphological aspects and distribution of fluid inclusions in quartz and cassiterite crystals. (A) Macroscopic feature of mineralized mica-quartz greisen from the Faixa Placha ore site. Note the fields with fluid inclusions studied; (B) cassiterite with demarcated fragmentation. (C) Microscopic features of the biphasic and monophasic pseudo-secondary fluid inclusions in cassiterite; (D) detailed sketch of fluid inclusions in cassiterite; (E) microscopic features of the biphasic and monophasic pseudo-secondary fluid inclusions in quartz; and (F) detailed sketch of fluid inclusions in quartz.

NaCl eq. (Fig. 9B), by applying an equation proposed by Bodnar (1993). Finishing with the total homogenization temperature (Tht), which varies from 255 to 270°C (Fig. 9C), marked by contraction of the gas phase until blending into the liquid phase (Liq. + Gas → Liq.). We use the calculated salinity versus Tht obtained to calculate the fluid density between 0.87 and 0.92 g/cm^3 (Fig. 9D, by applying Bakker's 2003 equation);

- Quartz: The Te occurs between -26.4 and -21.6°C, suggesting the presence of Na and K ions, as well as SO_4 and CO_3 molecules in this aqueous solution (Shepherd *et al.* 1985, Bodnar 1993, Bodnar and Vityk 1994). The Tmi occurred between -6.8 and -5.1°C (Fig. 9A), indicating a calculated salinity between 10.2 and 7.9 wt.% NaCl eq. (Fig. 9B), also applying Bodnar's (1993) equation. The Tht ranged from 108 to 214°C (Fig. 9C), also measured upon phase change Liq. + Gas → Liq. The calculated density varied from 0.92 to 1.0 g/cm^3 (Fig. 9D, also by applying Bakker's 2003 equation).

These microthermometric data reveal an aqueous fluid system with lowered salinity and density, trapped under low to moderate temperature (108–270°C), contrary to oxygen isotope data that revealed temperatures above 400°C. The fluid inclusions studied here represent rebalanced solutions trapped during or just after nucleation and mineral growth.

The coexistence of liquid- and vapor-rich fluid inclusions in the same fluid inclusions assemblage (Figs. 8C–8F) may indicate the presence of some fluid immiscibility process, such as boiling (e.g., Ramboz *et al.* 1982, Bodnar *et al.* 1985, Loucks 2000, Bodnar 2003). However, this process type was not clear to us in this study. Furthermore, the pseudo-secondary fluid inclusions show different salinity and Tht values, clearly noted in the salinity versus Tht diagram (Fig. 9E), indicating different intervals of fluid trapping between quartz and cassiterite. This characteristic suggests different degrees/ratios of mixing fluids (e.g., hydrothermal/magmatic vs. meteoric), favoring the fluid rebalancing. The flattening and mineral recrystallization features mostly seen in quartz also suggest that important fluid volume may have been trapped during the Faixa Placha reactivation phases, related to Brasiliano/Pan-African Orogeny.

DISCUSSION

Sn ± (W, Nb, Ta, REE) deposits are normally associated with the late magmatic-hydrothermal phase related to volatiles-rich highly fractionated granite evolution (Taylor 1979, Lehmann 1982, 2021, Strong 1985, Marignac and Cuney 1991, Taylor and Wall 1992, Burnham 1997, Sharma and Srivastava 2014, Audétat 2019). Its genesis requires specific physical-chemical parameters (temperature, pressure, pH, Eh, and fO_2) to control the metal extraction, transport, and precipitation phases during magmatic evolution. In this context, pegmatite, greisen, breccias, and veins-veinlets appear as the main ore deposition sites (Groves and McCarthy 1978, Pollard and Taylor 1986, Stemprok 1987, Heinrich 1990, Wood and Samson 1998, Černý and Ercit 2005).

Greisen results from a complex metasomatic process related to fluid phase exsolved from the residual melt at the final-stage magmatic evolution. Its genesis requires H_2O-CO_2-CH_4-salts solutions, temperature = 200–500°C, depth = 2–5 km, neutral to alkaline (pH = 6–8 or pH ≥ 8) environment, F-Cl halogen complexes action for metals transport, Fe-micas and feldspar leaching, followed by quartz, F-Li micas, fluorite, topaz, tourmaline, and Ca-Fe carbonates precipitation (Shcherba 1970, Burt 1981, Hedenquist and Lowenstern 1984, Stemprok 1987, Pollard *et al.* 1988). The forceful intrusions normally lead to subvertical tensile fractures/fissures bodies' propagation at the granitic cupula zone, favoring hydrothermal circulation, pressure, and temperature relaxation, followed by ore sites formation (Plimer 1987, Pirajano 1992, Launay *et al.* 2021). However, the cassiterite±wolframite content (Sn > W, Sn ≈ W, Sn < W) in these sites, in addition to the physical-chemical parameters mentioned above, also depends on some geological conditions, such as complexing element-type in metal transport, fluid-rock interaction rate, and different Sn-W partition coefficients in magmatic fractionation (Manning and Henderson 1984, Jackson and Helgeson 1985, Heinrich 1990).

The Sn (±W) greisen bodies found in the Bacia zone and Faixa Placha of the Pedra Branca granite massif are linked to highly fractionated Li-mica leucogranite magmatic phase (1.74 Ga) or pb2d petrographic type (Botelho 1992). In this metallogenetic framework, the forceful to passive magma emplacement favored fractures and faults generation at the cupula granitic zone, followed by a hydrothermal recirculation convective process that led to greisenization at the contact zone and dilated sites (fractures and faults), thus forming endo- to exogreisen related to the Bacia zone and Faixa Placha (Fig. 10), respectively. In these greisen bodies, the higher content of cassiterite in relation to wolframite (Sn >> W), as well as high content of ilmenite, magnetite, and hematite, indicates the predominance of the oxidizing environment during the greisenization phase. However, some oscillations in the hydrothermal oxidation state may have favored the precipitation of wolframite and S-minerals under a reduced condition.

The oxygen isotope ($\delta^{18}O$) data point to a crystallization temperature between 485 and 410°C, marked by an important isotopic fractionation process (quartz-cassiterite-water) during greisenization, which is linked to the lowering of temperature and the interaction between fluids from different sources (e.g., Taylor Jr. 1974, Taylor and Wall 1993, Zhang *et al.* 1994). The progressive changes in physical-chemical parameters (mainly temperature, pH,

Table 4. Summary of microthermometric intervals obtained on fluid inclusions from quartz and cassiterite crystals.

Host mineral	Eutectic temperature (°C)	Ice melting temperature (°C)	Total homogenization temperature (°C)	Salinity (%wt. NaCl eq)	Density (g/cm^3)
Cassiterite	-22.3 to -36.4	-8.2 to -10.4	255.1–268.9	11.9–14.4	0.87–0.92
Quartz	-21.6 to -26.4	-5.1 to -6.8	107.8–213.9	7.9–10.2	0.92–1.0

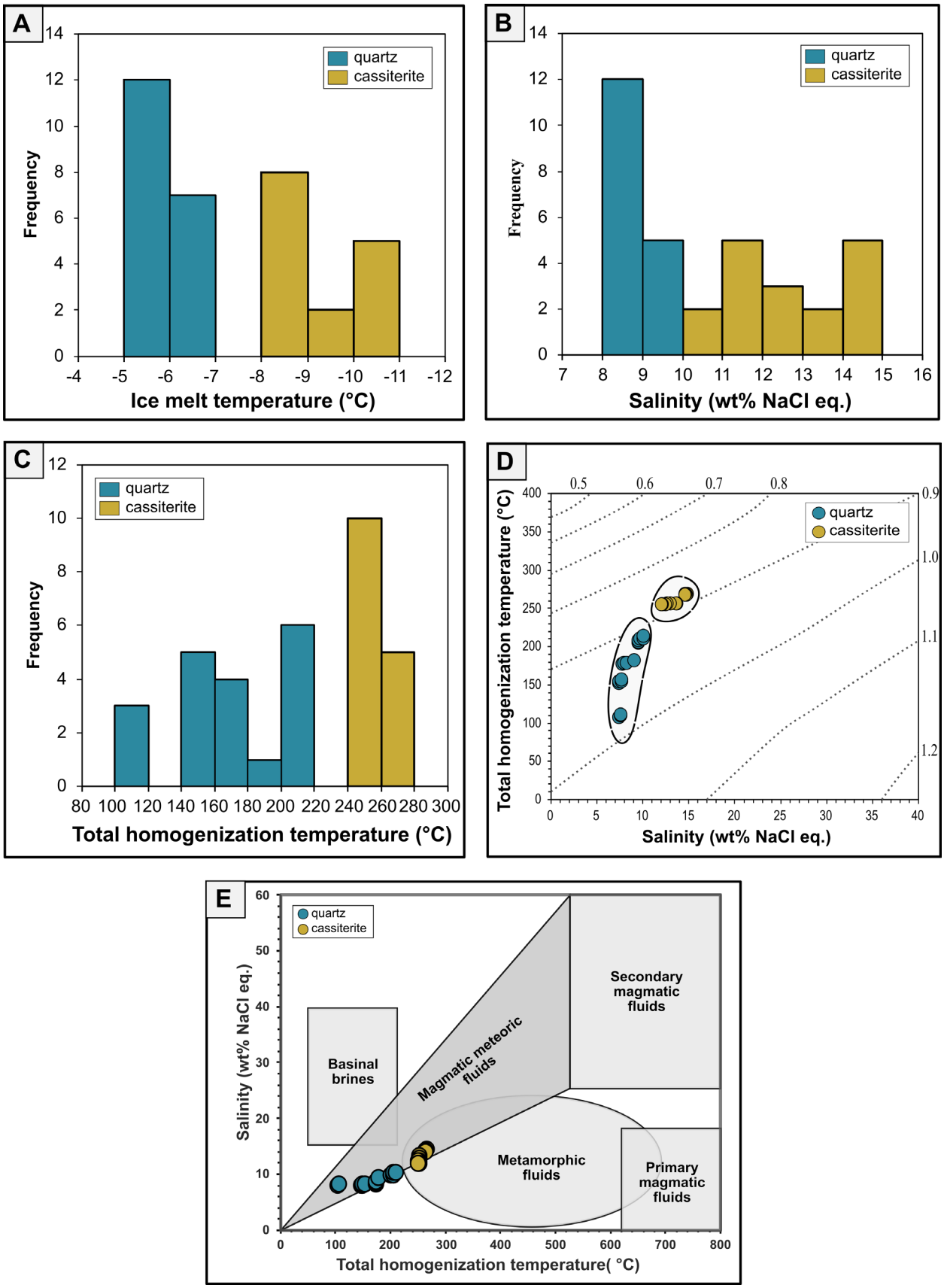

Figure 9. Histograms and graphs showing the microthermometric data obtained for fluid inclusions in cassiterite and quartz. (A) Histogram with the ice melting temperature; (B) histogram with the calculated salinities for ice melt temperature; (C) histogram with the total homogenization temperature (Tht); (D) total homogenization temperature versus salinity diagram indicating density fields generated by the equation of state by Zhang and Frantz (1987), obtained by Wilkinson (2001) from Brown (1989); (E) total homogenization temperature versus salinity diagram indicating a possible mixing trend field for the aqueous fluid system studied here (Sharma and Srivastava 2014).

Eh, and fO_2) on the hydrothermal system played an important role on the zoning and exsolution features identified in the cassiterite and wolframite, marked by different types of substitution controlling the entry of Fe, Ti, Mn, Nb, Ta, U, and In.

The growth and zoning of cassiterite crystals had $2Sn^{4+} + O^{2+} \leftrightarrow Ti^{4+} + Fe^{3+} + OH^-$ as the main replacement mechanism, followed by the entry of Nb, Ta, and In impurities, according to $2(Sn, Ti)^{4+} \leftrightarrow (Nb, Ta)^{5+} + (Fe, In)^{3+}$ equation, under an oxidizing environment. However, some oscillations in the oxidizing environment ($Fe^{3+} \leftrightarrow Fe^{2+}$), often linked to hydrothermal re-circulation convective, would have favored the entry of W, Mn, and U impurities, according to $2(Sn, Ti)^{4+} \leftrightarrow (W, Mn)^{6+} + Fe^{2+}$ or $2(Sn, Ti)^{4+} \leftrightarrow U^{4+} + 2Fe^{2+}$ equations. On the contrary, the wolframite growth had $Fe^{2+} + W^{6+} \leftrightarrow Fe^{3+} + (Nb, Ta)^{5+}$ as the main replacement mechanism, which may have been accompanied by oscillations of the hydrothermal oxidation state ($Fe^{2+} \leftrightarrow Fe^{3+}$) that favored to Nb + Ta increases, as well as the incorporation of some impurities (Sn^{4+}, In^{3+}, and U^{4+}). In this context, the high calculated Fe^{2+} values (Table 2), associated with the presence of S-minerals and U^{4+}, may indicate that the wolframite from the Faixa Placha ore site could also have been precipitated under reduced hydrothermal conditions (Hsu 1976, Heinrich 1990). According to Hsu (1976) and Ivanova (1988), Fe-rich wolframite is stable under oxidizing conditions at temperatures above 400°C. Therefore, it is possible that impurities identified in the wolframite are also linked to exsolution process during the lowering of the temperature.

Additionally, the U anomalous contents identified in cassiterite crystals from some granite-pegmatites of the Paranã subprovince (GTP) allowed obtaining U-Pb ages between 1.535 and 1.470 Ma (Sparrenberger and Tasinari 1999). The U content identified in cassiterite and wolframite from the Pedra Branca greisen could also be a good opportunity in the future to help in geochronological studies on the ore formation (e.g., Yuan *et al.* 2011, Li *et al.* 2016, Neymark *et al.* 2018, Li *et al.* 2022).

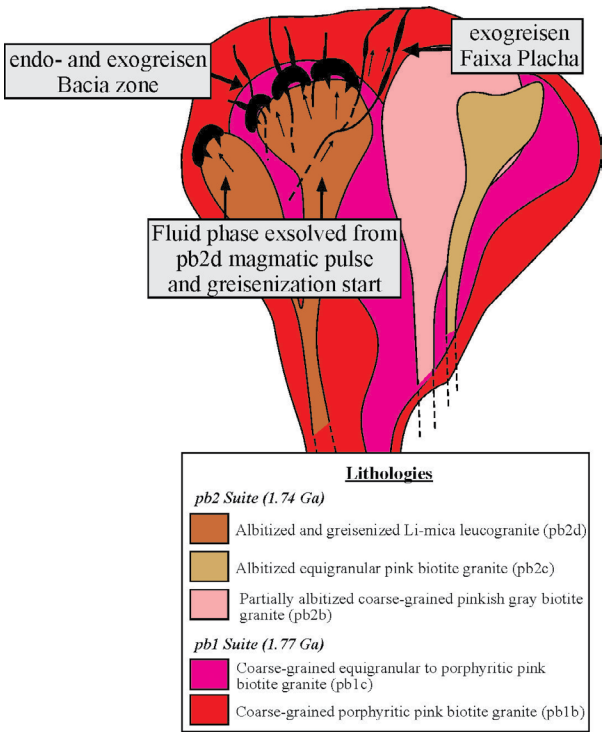

Figure 10. Proposed metallogenetic model for the mineralized greisen sites of the Pedra Branca granite massif.

During Neoproterozoic, nonetheless, the transpressive tectonics linked to Brasiliano/Pan-African Orogeny (800–500 Ma) printed different deformational stages in overall lithologies. The greisenized bodies and tensile faults/fractures filled by ore related to Faixa Placha (exogreisen), as well as some greisen lenticular bodies linked to Bacia zone (endo- and exogreisen), were then subjected to directional mylonitic deformation. Faixa Placha structures sets, above all, were reactivated under a ductile-ruptile regime, with local generation of centimetric folds, breccia, and tension gash, as well as flattening and partial fragmentation of the mineral assemblage. The recrystallization features are more common in quartz, whose fluid inclusions study revealed the dominant presence of low salinity aqueous solutions (H_2O-NaCl), probably channeled along the Faixa Placha during the Neoproterozoic shear at temperatures between 100 and 215°C. Aqueous solutions are also identified in broken cassiterite crystals, but with an increased salinity and total homogenization temperature range between 255 and 270°C, suggesting hydrothermal-magmatic systems involving recirculation of rebalanced aqueous solutions or immiscible aqueous fluid phase (e.g., Hulsbosch and Muchez 2020, Chen *et al.* 2021). However, fluid inclusions studies still need to advance on the ores of the Pedra Branca granite massif, in order to identify primary fluids with a thermal signature compatible with the oxygen isotope data presented here.

Finally, during Phanerozoic, the prolonged erosive process led to regional peneplanation, reaching the granitic cupolas and the surrounding wall rocks, carving relief in different intensities. The mineralized greisen zones present in the Bacia zone and Faixa Placha were then partially eroded, with their mineral components being channeled through the drainage system, and thus forming Sn (±W)-rich alluvium around the Pedra Branca granite massif.

CONCLUDING REMARKS

The set of information presented here leads us to the following conclusions about the Sn (±W) mineralization found in the Pedra Branca granitic massif (1.77–1.74 Ga).

The cassiterite and wolframite contents from the exogreisen Faixa Placha, linked to Li-mica leucogranite magmatic phase (1.74 Ga), were mainly deposited under oxidizing conditions at a temperature between 485 and 410°C. However, some oscillations in the oxidizing environment allowed the precipitation of S-minerals, as well as the entry of chemical impurities (e.g., Nb, Ta, In, and U) into the cassiterite and wolframite structures. This process favored to zoning and chemical variations during mineral growth, whose main substitution mechanisms can be expressed by the following equations:

- cassiterite = $2Sn^{4+} + O^{2+} \leftrightarrow Ti^{4+} + Fe^{3+} + OH^-$, accompanied by $2(Sn, Ti)^{4+} \leftrightarrow (Nb, Ta)^{5+} + (Fe, In)^{3+}$, $2(Sn,Ti)^{4+} \leftrightarrow (W, Mn)^{6+} + Fe^{2+}$ and $2(Sn, Ti)^{4+} \leftrightarrow U^{4+} + 2Fe^{2+}$ as coupled substitutions;
- wolframite = $Fe^{2+} + W^{6+} \leftrightarrow Fe^{3+} + (Nb, Ta)^{5+}$ and $2Fe^{2+} + W^{6+} \leftrightarrow 2(Fe, In)^{3+} + (Sn, U)^{4+}$.

The Neoproterozoic shear linked to Brasiliano/Pan-African Orogeny (800–500 Ma) reactivated the Faixa Placha and printed different deformational features and stages on the exogreisen that led to flattening and partial fragmentation of the mineral assemblage. According to fluid inclusion data, this process favored the recirculation of low salinity rebalanced aqueous solutions (H_2O-NaCl) at temperatures between 100 and 215°C channeled along the Faixa Placha.

ACKNOWLEDGMENTS

This research is the result of the Master's thesis presented by Santos I.K.M. (first author), which had financial support from the Brazilian National Council of Technological and Scientific Development (CNPq-Project n°443603/2014–6) and Coordination for the Improvement of Higher Education Personnel (CAPES) through scholarship. The authors are thankful to the EDEM — Development and Participations Mining Company — for fieldwork support. Thanks to Geosciences Institute and the Post-Graduate Program in Geology of the Universidade de Brasília (IGD-UnB) for the laboratorial infrastructure made available. Thanks also to the anonymous reviewers for the important contributions to the improvement of this manuscript. This research is linked to the study group named Granites and Associated Mineralizations (UnB-CNPq).

ARTICLE INFORMATION

Manuscript ID: 20220041. Received on: 08 JUN 2022. Approved on: 19 JAN 2023.

How to cite this article: Santos I.K.M., Souza V.S., Botelho N.F., Hoyer I.S., Bonfim L.A.R. 2023. Mineral chemistry and oxygen isotope studies on Sn (±W) mineralization from Pedra Branca Granite Massif, Central Brazil. *Brazilian Journal of Geology*, **53**(1):e20220041. https://doi.org/10.1590/2317-4889202320220041

Ítalo Kevin Morais dos Santos: Collection and investigation of material, methodology, formal analysis, validation, visualization, and writing — original draft. Valmir da Silva Souza: Project administration, collection and investigation of material, methodology, formal analysis, validation, visualization, supervision, and writing — original draft, review and editing. Nilson Francisquini Botelho: Project administration, collection and investigation of material, methodology, formal analysis, validation, visualization, supervision, and writing — original draft, review and editing. Ingrid de Souza Hoyer: Methodology, formal analysis, validation, visualization, and writing — original draft and review. Luis Antonio Raposo Bonfim: Collection and investigation of material and writing — original draft.

Competing interest: the authors declare no competing interests.

REFERENCES

Alderton D.H.M. 1989. Oxygen isotope fractionation between cassiterite and water. *Mineralogical Magazine*, **53**(371):373-376. https://doi.org/10.1180/minmag.1989.053.371.13

Almeida F.F.M., Hasui Y., Brito Neves B.B., Fuck R.A. 1981. Brazilian structural provinces: an introduction. *Earth Sciences Review*, **17**(1-2):1-29. https://doi.org/10.1016/0012-8252(81)90003-9

Alvarenga C.J.S., Botelho N.F., Dardenne M.A., Lima O.N.B., Machado M.A. 2007. *Mapa Geológico da Folha Cavalcante (SD.23-V-C-V), escala: 1.100.000*. Programa Levantamentos Geológicos Básicos do Brasil, Nota Explicativa Integrada com ds folhas Monte Alegre de Goiás (SD.23-V-C-III), Cavalcante (SD.23-V-C-V) e Nova Roma (SD.23-V-C-VI), Goiás. UnB/MME/CPRM, 67 p.

Audétat A. 2019. The metal content of magmatic-hydrothermal fluids and its relationship to mineralization potential. *Economic Geology*, **114**(6):1033-1056. https://doi.org/10.5382/econgeo.4673

Bakker R.J. 2003. Package FLUIDS 1. Computer programs for analysis of fluid inclusion data and for modelling bulk fluid properties. *Chemical Geology*, **194**(1-3):3-23. https://doi.org/10.1016/S0009-2541(02)00268-1

Bettencourt J.S., Leite Jr. W.B., Gorayeb C.L., Sparrenberger I., Bello R.M.S., Payolla B.L. 2005. Sn-polymetallic greisen-type deposits associated with late-stage rapakivi granites, Brazil: Fluid inclusion and stable isotope charactheristics. *Lithos*, **80**(1-4):363-386. https://doi.org/10.1016/j.lithos.2004.03.060

Bodnar R.J. 1993. Revised equation and table for determining the freezing point depression of H_2O-NaCl solutions. *Geochimica et Cosmochimica Acta*, **57**:683-684. https://doi.org/10.1016/0016-7037(93)90378-A

Bodnar R.J. 2003. Reequilibration of fluid inclusions. In: Samson I., Anderson A., Marshall D. (Eds.), *Fluid inclusions:* analysis and interpretation. Mineralogical Association of Canada, Short Course 32, p. 213-231.

Bodnar R.J., Reynolds T.J., Kuehn C.A. 1985. Fluid inclusion systematics in epithermal systems. Geology and geochemistry of epithermal systems: In: Berger B.R., Bethke P.M. (Eds.), *Reviews in Economic Geology*, v. 2, p. 73-97.

Bodnar R.J., Vityk M.O. 1994. Interpretation of microthermometric data for H_2O-NaCl fluid inclusions. In: De Vivo B., Frezzotti M.L. (Eds.), *Fluid inclusions in minerals:* Methods and application. Pontignsno: Siena, p. 117-130.

Botelho N.F. 1992. *Les ensembles granitiques subalcalins a peralumineux mineralise's en Sn et In de la Sous-Province Paranã, Etat de Goias, Brésil*. PhD Thesis, Université de Paris VI, France, 344 p.

Botelho N.F., Bilial E., Moutte J., Fonteilles M. 1993. Precambrian A-type tin-bearing granites in the Goiás Tin-Province, Central Brazil: a review. In: *Workshop Magmatismo Granítico e Mineralizações Associadas*. Academia Brasileira de Ciências. p. 5-8.

Botelho N.F., Marini O.J. 1984. Petrografia, petroquímica e transformações tardi/pós magmáticas do Granito Estanífero da Pedra Branca (GO). In: XXXIII Congresso Brasileiro de Geologia. *Anais*... Rio de Janeiro: SBG, v. 6, p. 2935-2949.

Botelho N.F., Marini O.J. 1985. As mineralizações de estanho do granito Pedra Branca – Goiás. In: II Simpósio de Geologia do Centro-Oeste. *Anais*... Goiânia: SBG, p. 107-119.

Botelho N.F., Moura M.A. 1998. Granite-ore deposit relationships in Central Brazil. *Journal of South American Earth Sciences*, **11**(5):427-438. https://doi.org/10.1016/S0895-9811(98)00026-1

Botelho N.F., Pimentel M.M. 1993. Geocronologia Rb-Sr das fases intrusivas do Maciço Granítico da Pedra Branca, Província Estanífera de Goiás. In: IV Congresso Brasileiro de Geoquímica. *Atas*... Brasília: SBGq, p. 253-255.

Botelho N.F., Rossi G. 1988. Depósito de estanho da Pedra Branca, Nova Roma, Goiás. In: *Principais depósitos brasileiros-metais básicos não ferrosos, ouro e alumínio*. Brasília: DNPM, v. 3, p. 267-285.

Brito Neves B.B, Fuck R.A., Pimentel M.M. 2014. The Brasiliano collage in south America: a review. *Brazilian Journal of Geology*, **44**(3):1-34. https://doi.org/10.5327/Z2317-4889201400030010

Brown P.E. 1989. FLINCOR: A Computer Program for the Reduction and Investigation of Fluid-Inclusion Data. *American Mineralogist*, **74**(11-12):1390-1393.

Burnham C.W. 1997. Magmas and hydrothermal fluids. In: Barnes H.L. (Ed.), *Geochemistry of Hydrothermal Ore Deposits*. 3rd ed. New York: John Wiley and Sons, p. 63-123.

Burt D.M. 1981. Acidity-salinity diagrams: applications to greisen and porphyry deposits. *Economic Geology*, **76**(4):832-843. https://doi.org/10.2113/gsecongeo.76.4.832

Carvalhêdo A.L.C., Carmelo A.C., Botelho N.F. 2020. Geophysical-geological model of the Pedra Branca massif in the Goiás Tin Province, Brazil. *Journal of South American Earth Sciences*, **101**:102593. https://doi.org/10.1016/j.jsames.2020.102593

Černý P., Ercit T.S. 2005. The classification of granitic pegmatites revisited. *The Canadian MIneralogist*, **43**(6):2005-2026. https://doi.org/10.2113/gscanmin.43.6.2005

Chang J., Li J-W, Audétat A. 2018. Formation and evolution of multistage magmatic-hydrothermal fluids at the Yulong porphyry Cu-Mo deposit, eastern Tibet: Insights from LA-ICP-MS analysis of fluid inclusions. *Geochimica et Cosmochimica Acta*, **232**:181-205, https://doi.org/10.1016/j.gca.2018.04.009

Chen Y., Wang Z., Li J. 2021. Ore-forming fluid evolution in the Giant Gejiu Sn–Cu polymetallic ore field, SW China: evidence from fluid inclusions. *Frontiers in Earth Science*, **9**:655777. https://doi.org/10.3389/feart.2021.655777

Clayton R.N., O'Neil J.R., Mayeda T.K. 1972. Oxygen isotope exchange between quartz and water. *Journal of Geophysical Research*, **77**(17):3057-3067. https://doi.org/10.1029/JB077i017p03057

Costa N.O., Botelho N.F., Garnier J. 2020. Concentration of rare earth elements in the Faixa Placha tin deposit, Pedra Branca A-Type Granitic Massif, central Brazil, and its potential for ion-adsorption-type REE-Y mineralization. *Ore Geology Reviews*, **123**:103606, https://doi.org/10.1016/j.oregeorev.2020.103606

Costi H.T., Horbe A.M.C., Borges R.M.K., Dall'Agnol R., Rossi A., Sighnolfi G. 2000. Mineral chemistry of cassiterites from Pitinga Province, Amazonian Craton, Brazil. *Revista Brasileira de Geociências*, **30**(4):775-782.

CPRM. 2007. *Geologia da folha Monte Alegre de Goiás (SD.23-V-C-23, escala 1:100.000)*. In: Série Programa Geologia do Brasil, Levantamentos Geológicos Básicos em SIG. Brasília: MME/CPRM/UnB, 67 p.

Crowe D.E., Riciputi L.R., Bezenek S., Ignatiev A. 2001. Oxygen isotope and trace element zoning in hydrothermal garnets: Windows into large-scale fluid-flow behavior. *Geology*, **29**(6):479-482. https://doi.org/10.1130/0091-7613(2001)029%3C0479:OIATEZ%3E2.0.CO;2

Daele J.V., Hulsbosch N., Dewaele S., Boiron M.-C., Piessens K, Boyce A., Muchez Ph. 2018. Mixing of magmatic-hydrothermal and metamorphic fluids and the origin of peribatholitic Sn vein-type deposits in Rwanda. *Ore Geology Reviews*, **101**:481-501. https://doi.org/10.1016/j.oregeorev.2018.07.020

Fallick A.E., Macaulay C.I., Haszeldine R.S. 1993. Implications of linearly correlated oxygen and hydrogen isotopic compositions and illite in the Magnus sandstone, North Sea. *Clays and Clay Minerals*, **41**(2):184-190. https://doi.org/10.1346/CCMN.1993.0410207

Faure G., Mensing T.M. 2004. *Isotopes:* principles and applications. 3rd ed. New York: John Wiley and Sons, 897 p.

Fuck R.A., Dantas E. L., Pimentel M.M., Botelho N. F., Armstrong R., Laux J.H., Junges S.L., Soares J.E., Praxedes I.F. 2014. Paleoproterozoic crust-formation for Atlantic supercontinent reconstruction. *Precambrian Research*, 244:53-74.

Fuck R.A., Pimentel M.M., Alvarenga C.J.S., Dantas E.L. 2017. The northern Brasília belt. In: Heilbron M., Cordani U., Alkmim F. (Eds.), *São Francisco Craton, Eastern Brazil*. Regional Geology Reviews. Springer, p. 205-220.

Giuliani G. 1987. La cassitérite zonée du gisement de Sokhret Allal (Granite des Zaer, Maroc Central): Composition chimique et phases fluid associées. *Mineralium Deposita*, **22**(4):253-261. https://doi.org/10.1007/BF00204517

Groves D.I., McCarthy T.S. 1978. Fractional crystallization and the origin of tin deposits in granitoids. *Mineralium Deposita*, **13**(1):11-26. https://doi.org/10.1007/BF00202905

Harlaux M., Mercadier J., Marignac C., Peiffert C., Cloquet C., Cuney M. 2018. Tracing metal sources in peribatholitic hydrothermal W deposits based on the chemical composition of wolframite: The example of the Variscan French Massif Central. *Chemical Geology*, **479**:58-85. https://doi.org/10.1016/j.chemgeo.2017.12.029

Hedenquist J.W., Lowenstern J.B. 1984. The role of magmas in the formation of hydrothermal ore deposits. *Nature*, **370**:519-527. https://doi.org/10.1038/370519a0

Heinrich C.A. 1990. The chemistry of hydrothermal tin(-tungsten) ore deposition. *Economic Geology*, **85**(3):457-481. https://doi.org/10.2113/gsecongeo.85.3.457

Heinrich C.A., Walshe J.L., Harrold B.P. 1996. Chemical mass transfer modelling of ore-forming hydrothermal systems: Current practice and problems. *Ore Geology Reviews*, **10**(3-6):319-338. https://doi.org/10.1016/0169-1368(95)00029-1

Hsu L.C. 1976. The stability relations of the wolframite series. *American Mineralogist*, **61**(9-10):944-955.

Hulsbosch N., Muchez P. 2020. Tracing fluid saturation during pegmatite differentiation by studying the fluid inclusion evolution and multiphase cassiterite mineralisation of the Gatumba pegmatite dyke system (NW Rwanda). *Lithos*, **354-355**:105285. https://doi.org/10.1016/j.lithos.2019.105285

Ivanova G. 1988. Geochemical conditions of formation of various composition wolframites. *Bulletin of Mineralogy*, **111**(1):97-103. https://doi.org/10.3406/bulmi.1988.8074

Jackson K.J., Hegelson H.C. 1985. Chemical and thermodynamic constraints on the hydrothermal transport and deposition of tin: I. Calculation of the solubility of cassiterite at high pressures and temperatures. *Geochimica et Cosmochimica Acta*, **49**(1):1-22. https://doi.org/10.1016/0016-7037(85)90187-5

Jacobi P. 2003. *A descoberta do depósito estanífero da Pedra Branca em Nova Roma/GO*. Available at: www.geologo.com.br/pedrabranca.asp. Accessed on: Mar 14, 2023.

Kelly W.C., Rye R.O. 1979. Geologic, fluid inclusion, and stable isotope studies of the tin-tungsten deposits of Panasqueira, Portugal. *Economic Geology*, **74**(8):1721-1822. https://doi.org/10.2113/gsecongeo.74.8.1721

Launay G., Sizaret S., Lach P., Melleton J., Gloaguen E., Poujol M. 2021. Genetic relationship between greisenization and Sn-W mineralizations in vein and greisen deposits: Insights from the Panasqueira deposit (Portugal). *Earth Sciences Bulletin of France*, **192**(1):2. https://doi.org/10.1051/bsgf/2020046

Lehmann B. 1982. Metallogeny of tin; magmatic differentiation versus geochemical heritage. *Economic Geology*, **77**(1):50-59. https://doi.org/10.2113/gsecongeo.77.1.50

Lehmann B. 2021. Formation of tin ore deposits: A reassessment. *Lithos*, **402-403**:105756. https://doi.org/10.1016/j.lithos.2020.105756

Lenharo S.R.L., Moura M.A, Botelho N.F. 2002. Petrogenetic and mineralization processes in Paleo- to Mesoproterozoic rapakivi granites: examples from Pitinga and Goiás, Brazil. *Precambrian Research*, **119**(1-4):277-299. https://doi.org/10.1016/S0301-9268(02)00126-2

Li C., Zhang R., Ding X., Ling M., Fan W., Sun W. 2016. Dating cassiterite using laser ablation ICP-MS. *Ore Geology Reviews*, **72**(Part 1):313-322. https://doi.org/10.1016/j.oregeorev.2015.07.016

Li J., Huang X., Fu Q., Li W. 2021. Tungsten mineralization during the evolution of a magmatic hydrothermal system: Mineralogical evidence from the Xihuashan rare-metal granite in South China. *American Geologist*, **106**(3):443-460. https://doi.org/10.2138/am-2020-7514

Li Y., He S., Zhang R.-Q., Bi X.-W., Feng L.-J., Tang G.-Q., Wang W.-Z., Huang F., Li X.-H. 2022. Cassiterite oxygen isotopes in magmatic-hydrothermal systems: in situ microanalysis, fractionation factor, and applications. *Mineralium Deposita*, 57:643-661. https://doi.org/10.1007/s00126-021-01068-x

Linnen R.L., Williams-Jones A.E. 1995. Genesis of a magmatic metamorphic hydrothermal system: The Sn-W Polymetallic deposits at Pilok, Thailand. *Economic Geology*, **90**(5):1148-1166. https://doi.org/10.2113/gsecongeo.90.5.1148

Loucks R.R. 2000. Precise geothermometry on fluid inclusion populations that trapped mixtures of immiscible fluids. *American Journal of Science*, **300**(1):23-59. https://doi.org/10.2475/ajs.300.1.23

Macaulay C.I., Fallick A.E., Haszeldine R.S., Graham C.M. 2000. Methods of laser-based isotope measurement applied to diagenetic and hydrocarbon reservoir quality. *Clay Minerals*, **35**(1):313-322. https://doi.org/10.1180/000985500546684

Macavei J., Schulz H. 1993. The crystal structure of wolframite type tungstates at high pressure. *Zeitschrift fur Kristallographie*, **207**(2):193-208. https://doi.org/10.1524/zkri.1993.207.Part-2.193

Macey P., Harris C. 2006. Stable isotope and fluid inclusion evidence for the origin of the Brandberg West area Sn–W vein deposits, NW Namibia. *Mineralium Deposita*, **41**:671-690. https://doi.org/10.1007/s00126-006-0079-1

Manning D.A.C., Henderson P. 1984. The behaviour of tungsten in granitic melt-vapour systems. *Contributions to Mineralogy and Petrology*, **86**(3):286-293. https://doi.org/10.1007/bf00373674

Marignac C., Cuney M. 1991. What is the meaning of granite specialization for Sn, W deposit genesis? In: Pagel M., Leroy J.L. (Eds.), *Source, transport and deposition of metals*. Rotterdam, Balkema, p. 771-774.

Marini O.J., Botelho N.F. 1986. A província de granitos estaníferos de Goiás. *Revista Brasileira de Geociências*, **16**:119-131.

Marini O.J., Botelho N.F., Rossi P. 1992. Elementos Terras Raras em granitóides da Província Estanífera de Goiás. *Revista Brasileira de Geociências*, **22**(1):61-72.

Martins-Ferreira M.A.C. 2019. Effects of initial rift inversion over fold-and-thrust development in a cratonic far-foreland setting. *Tectonophysics*, **757**:88-107. https://doi.org/10.1016/j.tecto.2019.03.009

Mering J.A., Barker S.L.L., Huntingston K.W., Simmons S., Dipple G. 2018. Taking the temperature of hydrothermal ore deposits using clumped isotope thermometry. *Economic Geology*, **113**(8):1671-1678. https://doi.org/10.5382/econgeo.2018.4608

Möller P., Dulski P., Szacki W., Malow G., Riedel E. 1988. Substitution of tin in cassiterite by tantalum, niobium, tungsten, iron and manganese. *Geochimica et Cosmochimica Acta*, **52**(6):1497-1503. https://doi.org/10.1016/0016-7037(88)90220-7

Murciego A., Sanchez A.G., Dusausoy Y., Pozas J.M.M., Ruck R. 1997. Geochemistry and EPR of cassiterites from the Iberian Hercynian Massif. *Mineralogical Magazine*, **61**(3):357-365.

Nascimento T.M.F., Souza V.S. 2017. Mineralogy, stable isotopes ($\delta^{18}O$ and $\delta^{34}S$) and ^{40}Ar-^{39}Ar geochronology studies on the hydrothermal carapace of the Igarapé Manteiga W-Sn Deposit, Rondônia. *Brazilian Journal of Geology*, **47**(4):591-613. https://doi.org/10.1590/2317-4889201720170068

Neiva A.M.R. 1996. Geochemistry of cassiterite and its inclusions and exsolutions products from tin and tungsten deposits in Portugal. *The Canadian Mineralogist*, **34**(4):745-768.

Neiva A.M.R. 2008. Geochemistry of cassiterite and wolframite from tin and tungsten quartz veins in Portugal. *Ore Geology Reviews*, **33**(3-4):221-238. https://doi.org/10.1016/j.oregeorev.2006.05.013

Neymark L.A., Holm-Denoma C.S., Moscati R.J. 2018. In situ LA-ICPMS U-Pb dating of cassiterite without a known-age matrix-matched reference material: Examples from worldwide tin deposits spanning the Proterozoic to the Tertiary. *Chemical Geology*, **438**:410-435. https://doi.org/10.1016/j.chemgeo.2018.03.008

Padilha J.L., Laguna A.M.G. 1981. Geologia dos granitos da Pedra Branca, Mocambo, Mangabeira e Serra do Mendes – Goiás. In: I Simpósio de Geologia do Centro-Oeste. *Atas*... Goiânia: SBG, p. 622-643.

Pimentel M.M. 2016. The tectonic evolution of the neoproterozoic Brasília Belt, central Brazil: a geochronological and isotopic approach. *Brazilian Journal of Geology*, **46**(Suppl. 1):67-82. https://doi.org/10.1590/2317-4889201620150004

Pimentel M.M., Heaman L., Fuck R.A., Marini O.J. 1991. U-Pb zircon geochronology of Precambrian tin-bearing continental-type acid magmatism in central Brazil. *Precambrian Research*, **52**(3-4):321-335. https://doi.org/10.1016/0301-9268(91)90086-P

Pirajano F. 1992. Greisen systems. In: Hydrothermal mineral deposits: principles and fundamental concepts for the exploration geologist. Berlin: Springer, v. 9, p. 280-324. https://doi.org/10.1007/978-3-642-75671-9_10

Plimer I.R. 1987. Fundamental parameters for the formation of granite-related tin deposits. *Geologische Rundschau*, **76**(1):23-40. https://doi.org/10.1007/BF01820571

Pollard P.J., Taylor R.G. 1986. Progressive evolution of alteration and tin mineralization: Controls by interstitial permeability and fracture-related tapping of magmatic fluid reservoirs in tin granites. *Economic Geology*, **81**(7):1795-1800. https://doi.org/10.2113/gsecongeo.81.7.1795

Pollard P.J., Taylor R.G., Cuff C. 1988. Genetic modelling of greisen-style tin systems. In: Hutchison C.S. (ed.), *Geology of Tin Deposits in Asia and the Pacific*. Berlin, Heidelberg: Springer, p. 59-72. https://doi.org/10.1007/978-3-642-72765-8_3

Polya D.A. 1988. Compositional variation in wolframites from the Barroca Grande mine, Portugal: Evidence for fault-controlled ore formation. *Mineralogical Magazine*, **52**(367):497-503. https://doi.org/10.1180/minmag.1988.052.367.08

Ramboz C., Pichavant M., Weisbord A. 1982. Fluid immiscibility in natural process: use and misuse of fluid inclusion data (II. Interpretation of fluid inclusion data in terms of immiscibility). *Chemical Geology*, **37**(1-2):29-48. https://doi.org/10.1016/0009-2541(82)90065-1

Roedder E. 1984. Fluid inclusions. In: *Reviews in Mineralogy*. Mineralogical Society of America, v. 12, p. 644.

Shcherba G.N. 1970. Greisens (part 1). *International Geology Review*, **12**(2):114-255.

Sharma R., Srivastava P.K. 2014. Hydrothermal fluids of magmatic origin. In: Kumar S., Singh R.N. (Eds.), *Modelling of magmatic and allied processes*. Society of Earth Scientists Series, p. 181-208. https://doi.org/10.1007/978-3-319-06471-0_9

Sharp Z.D., Gibbons J.A., Maltsev O., Atudorei V., Pack A., Sengupta S. 2016. A Calibration of the Triple Oxygen Isotope Fractionation in the SiO_2 -H_2O System and Applications to Natural Samples. *Geochimica et Cosmochimica Acta*, **186**:105-119. https://doi.org/10.1016/j.gca.2016.04.047

Shepherd T.J., Rankin A.H., Alderton D.H.M.A. 1985. *A practical guide to fluid inclusion studies*. New York: Blackie & Son, 239 p.

Silva C.C., Souza V.S. Botelho N.F., Dantas E.L. 2021. Contribution to petrogenesis of the Paleoproterozoic basaltic magmatism from the Araí continental rift, central Brazil. *Journal of South American Earth Sciences*, **110**:103345. https://doi.org/10.1016/j.jsames.2021.103345

Souza V.S., Botelho N.F. 2009. Composição química e isótopos de oxigênio em cassiterite e wolframita nos greisens do albita granito Palanqueta, depósito de estanho de Bom Futuro (RO). *Revista Brasileira de Geociências*, **39**(4):695-704.

Sparrenberger I., Tassinari C.C.G. 1999. Subprovíncia do Rio Paranã (GO): um exemplo de aplicação dos métodos de datação U-Pb e Pb-Pb em cassiterita. *Revista Brasileira de Geociências*, **29**(3):405-414.

Stemprok M. 1987. Greisenization (a review). *Geological Rundschau*, **76**(1):169-175. https://doi.org/10.1007/BF01820580

Strong D.F. 1985. A review and model for granite-related mineral deposits. In: Taylor R.P., Strong D.F. (Eds.), *Recent advances in the geology of granite-related mineral deposits*. The Canadian Institute of Mining and Metallurgy (Special Volume), v. 39, p. 424-445.

Sun S.S., Eadington P.J. 1987. Oxygen isotope evidence for the mixing of magmatic and meteoric waters during tin mineralization in the Mole granite, New South Wales, Australia. *Economic Geology*, **82**(1):43-52. https://doi.org/10.2113/gsecongeo.82.1.43

Tanizaki M.L.N., Campos J.E.G., Dardenne M.A. 2015. Estratigrafia do Grupo Araí: registro de rifteamento paleoproterozóico no Brasil Central. *Brazilian Journal of Geology*, **45**(1):95-108. https://doi.org/10.1590/2317-4889201500010007

Taylor R.G. 1979. Geology of tin deposits. In: *Developments in economic geology* (11). Amsterdam: Elsevier, 543 p.

Taylor J.R., Wall V.J. 1992. The behavior of tin in granitoid magmas. *Economic Geology*, **87**(2):403-420. https://doi.org/10.2113/gsecongeo.87.2.403

Taylor J.R., Wall V.J. 1993. Cassiterite solubility, tin speciation, and transport in magmatic aqueous phase. *Economic Geology*, **88**(2):437-460. https://doi.org/10.2113/gsecongeo.88.2.437

Taylor Jr. H.P. 1974. The application of oxygen and hydrogen isotope studies to problems of hydrothermal alteration and ore deposition. *Economic Geology*, **69**(6):843-883. https://doi.org/10.2113/gsecongeo.69.6.843

Taylor Jr. H.P. 1997. Oxygen and hydrogen isotope relationships in hydrothermal mineral deposits. In: Barnes H.L. (Ed.), *Geochemistry of hydrothermal ore deposits*. 3rd ed. New York: John Wiley and Sons, p. 229-302.

Teixeira L.M. 2002. *Caracterização de minerais portadores de terras raras e sua aplicação à petrologia e geocronologia de granitos das subprovíncias Tocantins e Paranã – Goiás*. Tese de Doutorado, Instituto de Geociências, Universidade de Brasília, Brasília, 356 p.

Teixeira L.M., Botelho N.F. 1999. Comportamento dos elementos terras raras pesadas em zircão, xenotime e torita de granitos e greisens da subprovíncia estanífera Paranã, Goiás. *Revista Brasileira de Geociências*, **29**(4):549-556.

Teixeira L.M., Botelho N.F. 2002. Comportamento cristaloquímico de monazita primária e hidrotermal durante a evolução de granitos e greisens: exemplos das subprovíncias Tocantins e Paranã, Goiás. *Revista Brasileira de Geociências*, **32**(3):335-342.

Tindle A.G., Webb P.C. 1989. Niobian wolframite from Glen Gairn in the eastern Highlands of Scotland: A Microprobe investigation. *Geochimica et Cosmochimica Acta*, **53**(8):1921-1935. https://doi.org/10.1016/0016-7037(89)90313-X

Uhlein A., Fonseca M.A., Serr H.J., Dardenne M.A. 2012. Tectônica da Faixa de Dobramentos Brasília – setores setentrional e meridional. *Geonomos*, **20**(2):1-14. https://doi.org/10.18285/geonomos.v2i20.243

Valeriano C.M. 2017. The southern Brasília belt. In: Heilbron M., Cordani U., Alkminm F. (Eds.), *São Francisco Cráton, Eastern Brazil*. Regional Geology Reviews. Springer, p. 189-203.

Van den Kerkhof A.M., Hein U.F. 2001. Fluid inclusion petrography. Special volume in honor of Jacques Touret. In: Andersen T., Frezzotti M.L., Burke E.A.J. (eds.), *Fluid Inclusions:* Phase relationships methods applications. Lithos, v. 55, p. 27-47.

Waychunas G.A. 1991. Crystal chemistry of oxides and oxy-hydroxydes. In: Lindsley D.H. (ed.), Oxide minerals: petrologic and magnetic significance. Michigan: Mineralogical Society of America. *Reviews in Mineralogy*, **25**(2):11-68.

Wilkinson J.J. 2001. Fluid inclusions in hydrothermal ore deposits. *Lithos*, **55**(1-4):229-272. https://doi.org/10.1016/S0024-4937(00)00047-5

Wood S.A., Samson I.M. 1998. Solubility of ore minerals and complexation of ore metals in hydrothermal solution. In: Richards J.P., Larson P.B. (Eds.), Techniques in Hydrothermal Ore Deposits Geology. *Reviews in Economic Geology*, **10**(2):33-80.

Yang M., Yang Y.-H., Wu S.-T., Romer R.L., Che X.-D., Zhao Z.-F., Li W.-S., Yang J.-H., Wu F.-Y., Xie L.-W., Huang C., Zhang D., Zhang Y. 2020. Accurate and precise in situ U–Pb isotope dating of wolframite series minerals via LA-SF-ICP-MS. *Journal of Analytical Atomic Spectometry*, **35**(10):2191-2203. https://doi.org/10.1039/d0ja00248h

Yuan S.D., Peng J.T., Hao S., Li H.M., Geng J.Z., Zhang D.L. 2011. In situ LA-MC-ICP-MS and ID-TIMS- U-Pb geochronology of cassiterite in the Giant Furong tin deposit, Hunan Province, South China: New constraints on the timing of tin-polymetallic mineralization. *Ore Geology Reviews*, **43**(1):235-242. https://doi.org/10.1016/j.oregeorev.2011.08.002

Zhang L.-G., Liu J.-X., Chen Z.-S., Zhou H.-B. 1994. Experimental investigation of oxygen isotope fractionation in cassiterite and wolframite. *Economic Geology*, **89**(1):150-157. https://doi.org/10.2113/gsecongeo.89.1.150

Zhang Y.G., Frantz D. 1987. Determination of the homogenization temperatures and densities of supercritical fluids in the system NaCl-KCl-$CaCl_2$-H_2O using synthetic fluid inclusions. *Chemical Geology*, **64**(3-4):335-350. https://doi.org/10.1016/0009-2541(87)90012-X